Recent Developments in Low-Temperature Solution-Processed Metal Oxide Electron Transport Layers for Perovskite Solar Cells

Hafiz Muhammad Noman [a], Muhammad Tahir Hasan [a], Muhammad Anwar Jan [a], Muhammad Umair Ahsan Khan [a], Muhammad Jamshaid [a], Akbar Ali Qureshi [a *]
[a] Department of Mechanical Engineering, Bahauddin Zakariya University, 60000, Multan, Pakistan
[*]*Corresponding author*: akbaraliqureshi@bzu.edu.pk
Received: 21-09-2024, Received in Revised form: 04-10-2024, Accepted: 08-10-2024, Published: 30-12-2024

ABSTRACT

With power conversion efficiency (PCE) exceeding 25%, perovskite solar cells (PSC) have become known as a remarkable photovoltaic technology in the last few years. Further, the low preparation temperature and facile processing techniques specifically in the planar architecture have contributed immensely to the production of inexpensive solar devices. The charge transport layers, primarily the electron transport layer (ETL) play a significant role in efficient charge extraction and transport from the absorber layer to the respective electrode. In particular, numerous research have been carried out. On the oxides of metal (MOX) based ETL owing to their exceptional optoelectronic characteristics, low cost, and remarkable adaptability. This review deals with the application of newly developed MOX-based ETLs processed at low temperatures for planar PSC. The optical and electrical characteristics of widely used MOX ETL were briefly investigated and explored for impact on the photovoltaic (PV) stability and performance of halide PSC. In the end, the future perspective on the MOX ETL was also offered.

Keywords: Electron transport layer, metal oxides, optoelectronics, perovskite solar cell

Introduction

The biggest challenge to mankind in the next 50 years will be related to the energy crisis and environmental disorder [1]. Our industrialized civilization has an ever-increasing demand for energy and the only viable solution is fossil fuels which has already led to the depletion of the earth's oil reserves [2]. The global world is suffering due to energy-related problems and the possible remedial measure is to shift the dependence on sustainable and green energy resources [3]. In our daily lives, we use a variety of energy resources, including oil, coal, solar, and wind energy. Due to non-renewable energy resources, different kinds of pollutants and hazardous gasses are released into the atmosphere [4]. Numerous health issues arise from the use of fossil fuels. In addition, it produces pollution of the water, land, and air. Furthermore, it raises the temperature of the earth's surface and the atmosphere resulting in severe climate changes [5]. Therefore, to resolve these issues, alternative energy resources must be explored.

Solar, wind, and other forms of renewable energy resources are extensively investigated today to gain independence from fossil fuels in the future. One of the greatest sources of renewable energy is sun energy which is a limitless, environmentally benign, and cost-effective resource [6]. "In just one hour, the solar energy striking the planet is predominantly higher than the total energy utilized by humans in one year" [7]. The global energy demand can be overcome by the use of solar energy-based devices [8]. Numerous PV technologies have been discovered to date for effectively capturing solar energy and generating power. Perovskite solar cells, a developing superstar among them, are considered to be the most promising option due to their affordable fabrication cost, simplicity in manufacturing, and high power conversion efficiency (PCE) [9-11].

Through revolutionary advancement in the development of perovskite thin films with high crystalline nature, interfacial design, and device engineering, PSCs have attained a remarkable PCE of 26.5%, setting a new world record [12-14]. The rapid advancement in PCE of PSC is mainly attributed to exceptional optolectrical characteristics of perovskite material like large carrier diffusion length, low binding energy of exciton, greater light absorption capacity, and long carrier lifespans [15-17]. Miyasaka's team introduced $MAPbBr_3$ nanocrystalline thin-film as a sensitizer in a dye-sensitized solar cell (DSSC) in 2009 achieving a PCE of 3.8% [18]. However, these perovskite-sensitized solar cells exhibited bad photostability. Using electrolytes in liquid form critically degraded the perovskite films. Ever since Park et al. presented spiro-OMeTAD as a potential hole-carrying material and incredibly fabricated the first common solid-state PSC [19].

One of the most significant device architectures is the mesoporous solid-state perovskite solar cell. Unfortunately, the mesoporous TiO_2 often needs to be sintered at a high temperature. Of over 500 °C to enhance film characteristics and crystallinity [20]. High-temperature annealing and complex film formation processes limit its application in the fabrication of flexible devices [21]. The development of planar-type PSC can reduce the processing temperature and speed up the production process and is a distinctive technique for device fabrication with versatile compatibility [22-24]. Even in the absence of the mesoporous layer, the charge carriers (electrons and holes) can effectively travel to their respective electrodes due to the long carrier diffusion length and long carrier lifespan of the absorber material in planar architectures [25, 26]. The standard planar PSC can now be divided into two structural types: planar n-i-p (regular) and planar p-i-n (Inverted) illustrated in Figure 1a. In particular, ETLs are indispensable for the efficient collecting and transport of photogenerated electrons in planar PSC (Figure 1b), for blocking holes, and for reducing interfacial recombination [22-25]. In PSC, electron transport material (ETM) mostly utilized can be of organic or inorganic nature [27]. Organic ETLs excel in both flexibility and better solution processes [28]. Yet, they suffer from high costs and manifest deprived thermo-mechanical and environmental stability [29-31]. Inorganic n-type substances, particularly MO_X like titanium dioxide, zinc oxide, tin oxide, and iron oxide are frequently employed ETLs owing to their superior optoelectronic properties, facile solution processed techniques, low annealing temperatures, tremendous adaptability, and high stability [22-24, 32, 33]. Currently, a

lot of research is being carried out to explore novel ETL materials and improve MO_X ETLs to expand their application in PSC [34-36]. Various reviews on the development and progress of MO_X ETLs in PSC have been published, and a few of them have systematically concentrated on the MO_X ETLs processed at low temperatures in planar PSC [21, 37-39]. In this review, the electrical and optical properties of the popular MO_X ETLs TiO_2, ZnO, SnO_2, and α-Fe_2O_3 are discussed, followed by the impact of elemental doping and thin film formation. The latest developments in low-temperature processing of these MO_X ETLs for planar PSC are then reviewed. Lastly, a viewpoint on the challenges and bright future of MO_X ETLs processed at low temperatures is presented.

Metal Oxide as ETL Materials

Fundamental Characteristics of MO_X-based ETLs

The versatile optoelectronic properties of ETLs have an important impact on the photovoltaic solar cell performance. An important consideration is the energy level and the band gaps of the MO_X-based ETLs as shown in in Figs. 2a and 2b.

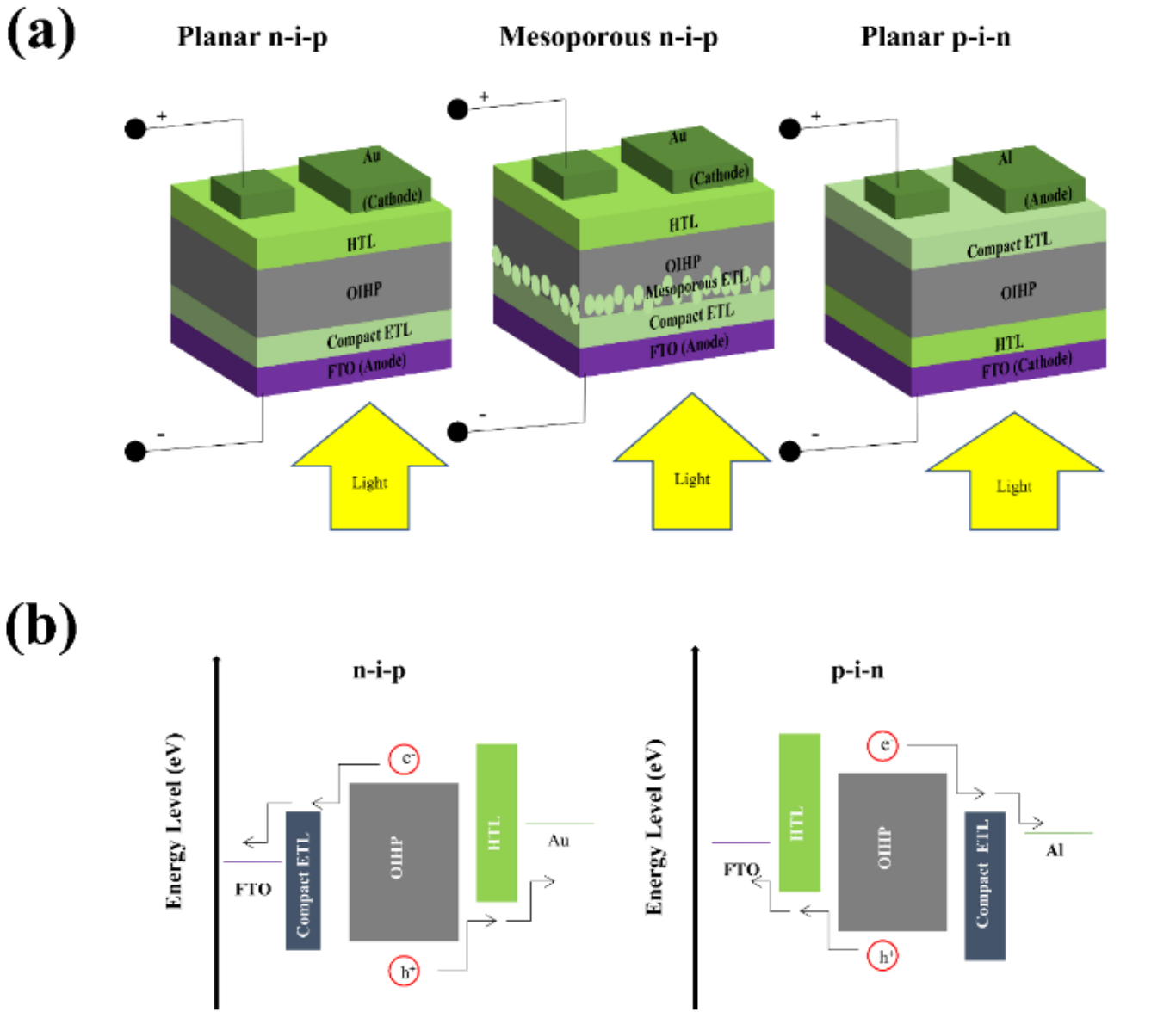

Figure 1. (a) Different configurations of a PSC including planar and mesoporous architectures; and (b) Energy level diagram of planar PSC.

.

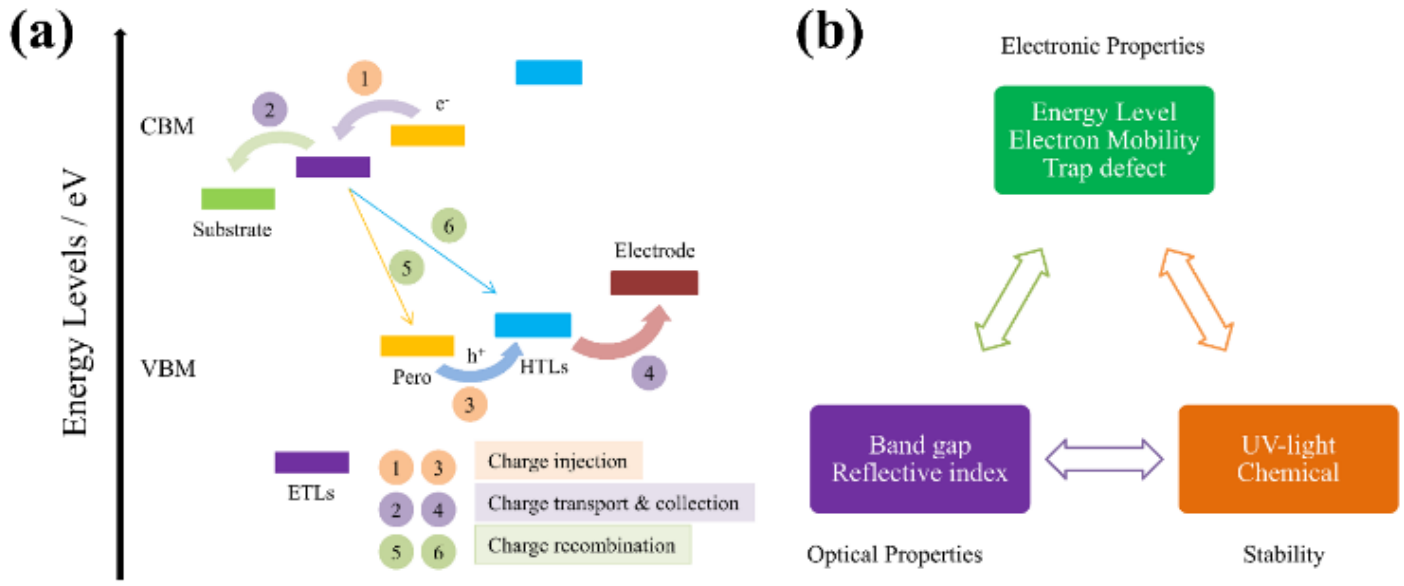

Figure 2. (a) Diagrammatic illustration of the charge transfer mechanism in standard PSC based on MO_X ETLs; and (b) fundamental performance influencing parameters for optimal MO_X ETLs.

To facilitate smooth electron extraction by effectively blocking the unwanted hole carriers, a perfect alignment of the band between the MO_X ETLs and the perovskite thin layer is desired [40]. Furthermore, for effective charge transfer and collection by lowering interfacial recombination and interface contact resistance, a fast electron mobility of the ETL is required. Wide band gap and low refractive index MO_X typically have favorable transmittance, which could increase the amount of sunlight that reaches the perovskite absorption layer in a typical PSC. To ensure the durability of the contact between ETLs and perovskite, MO_X ETLs on conductive substrates should also be UV-insensitive [41]. To prevent gradual interaction with the neighboring conductive electrode or perovskite film under certain circumstances, a MO_X ETL must possess strong chemical stability [42]

Among n-type MO_X, TiO_2, ZnO, SnO_2 and α-Fe_2O_3 are preferred ETLs for superior performance planar PSC. Due to the broader bandgap and appropriate energy levels with the absorber layer, TiO_2 is the most commonly used ETL in planar PSC and was previously utilized as a potential photoanode in DSSC [21]. The conduction band minimum (CBM) of TiO_2 is specifically located at -4.1 eV, with the band gaps for anatase, brookite, and rutile being 3.2 eV, 3.1 eV, and 3.0 eV, respectively [43, 44]. Moreover, it possesses a low index of refraction 2.4–2.5. But, TiO_2 suffers from low mobility of electrons from 0.1 $cm^2V^{-1}s^{-1}$ up to 4 $cm^2V^{-1}s^{-1}$ in bulk ranging [37]. The strong catalytic behavior of TiO_2 may cause deterioration of the perovskite layer under ultraviolet (UV) light [45]. Another common ETM that has gained interest as a substitute for TiO_2 is ZnO. ZnO is similar to TiO_2 due to its photoactive nature and possesses a fair energy level structure and a high visible light transmittance. Further, ZnO has a bulk electron mobility that is significantly higher than TiO_2 (> 200 cm^2 V^{-1} s^{-1}) [46-48]. ZnO also exhibits good structural tunability at the nanoscale. It can be easily crystallized to produce many kinds of nanocomposites at low temperatures, including nanoparticles, nanorods, and nanoflowers [37]. However, its application is restricted because of its poor chemical and thermal stability particularly at the ZnO/perovskite interface as a result of hydroxyl groups or left over acetate ligands on the ZnO surface [49]. SnO_2 has received substantial interest recently and is considered to be the most wonderful ETL due to its exceptionally high mobility of electrons and reasonably deep conduction band minimum ranging from -4.2 eV to -4.5 eV. Additionally, SnO_2 possesses a high transmittance across the complete visible spectrum, a large optical band gap, and a tiny refractive index [38, 50]. In contrast to all other ETLs, SnO_2 was notable for its low photo-catalytic activity, strong chemical stability, and resistance to UV light [50, 51]. The energy level alignment matching between MO_X ETL and the perovskite layer ensures efficient charge extraction without recombination loss. However, materials (e.g., SnO_2) with the conduction band level that can match the perovskite layer well but block hole transfer make it easy for electron injection into the perovskite layer and preventing a hole from injecting in from the anode side, thereby boosting device performance. Tin (Sn) scarcity of resources, however, is one of its main issues. According to a recent International Sn Association study, Sn availability is finite and advises researchers to search for an other metal. The study also demonstrates that Sn availability is already crucial in the US and China, it is about to become scarce in the EU as well [52]. Hematite (α-Fe_2O_3) is a thermodynamically stable n-type semiconducting iron oxide that has gained global attention due to its low UV photocatalytic activity that is useful for prolonging the UV stability of PSC [53]. However, MO_X still has some inherent issues like trap states, poor mobility, and low energy levels, despite their great potential for use as ETLs in PSC.

ETL	E_g/eV	CBM/eV	Refractive Index	Bulk Mobility /($cm^2.V^{-1}.S^{-1}$)	Ref.
TiO_2	3.0-3.2	-4.1	2.4-2.5	0.1-4	[37, 43, 44]
ZnO	3.1-3.3	-4.17	2.1	205	[38, 46-48]
SnO_2	3.6-4.0	-4.3	2.0	240	[37-39, 50]
WO_X	2.6-3.1	-4.5	1.95	10-20	[54-56]
Nb_2O_5	3.2-3.9	-4.25	2.1-2.4	0.2-0.4	[57-59]
Cr_2O_3	3.5	-3.93	1.4-2.1	10^{-5}-1	[60-62]
CeO_X	3.5	-4.0	1.6-2.5	0.01	[38, 63, 64]
Fe_2O_3	2.2	-4.5	2.7-3.5	0.01-0.1	[65-67]
Zn_2SnO_4	3.8	-4.1	2.0	10-30	[68, 69]
$BaSnO_3$	3.1	-4.3	2.07	50	[70-72]
$TiZn_2O_4$	3.29	-4.13	-	-	[73]
$Ti_{0.5}Fe_{0.5}O_X$	2.65	-4.08	-	-	[74]

Table 1

Comparison of electrical characteristics for binary and ternary MOx ETLs in planar Perovskite solar cell

Doping is widely used to adjust the physicochemical, optical, and electrical characteristics of MO_X [75]. In general, this technique could be beneficial in shifting the CB maxima to improve energy level alignment as well as passivate oxygen vacancies and decrease surface trap states of MO_X [49, 76]. Additionally, doping may also greatly improve electron transport and extraction from MO_X and increase its mobility. Surface modification is another useful strategy for improving electrical characteristics and minimizing surface flaws in MO_X [77, 78]. Furthermore, the development of new composites such as mixing MO_X directly with carbon materials or with another binary MO_X possessing prerequisite characteristics is beneficial in manipulating MO_X properties through synergistic effects. For example, SnO_2 layers decorated with graphene quantum dots (GQDs) enhanced film uniformity and conductivity. By manipulating the quantity and composition of GQDs, higher fermi levels were achieved, which considerably enhanced the transfer of electrons and device efficiency of a conventional PSC [79]. The electrical properties of ternary and binary MO_X ETLs that are often employed as ETL in planar PSC are shown in Table 1.

Techniques for Deposition of MO_X ETLs

Low-temperature solution-processed MO_X ETLs can be deposited on a perovskite absorber or conductive substrate in a PSC by a variety of methods. The properties of universal approaches are listed below.

Solution Process Method

Low-temperature ETLs are usually deposited using the solution-processed approach, which involves either directly producing MO_X nano-crystals and nano-colloidal or by thermal decomposition of the precursors of metal salt as displayed in Figure 3a [80-83]. To deposit a metal salt precursor on the substrate via the thermal decomposition technique, the precursors of metal salt are initially mixed with the suitable solvent and then deposited on glass conductive substrates by spin coating, spray coating,.etc. Thermal annealing was then conducted to transform the allocated films into the desired MO_X layers. The separation of the film formation and metal oxide crystallization enables direct coating of the resulting nano-sized solution using a range of conventional methods, including spin coating, slot die coating, and ink jet printing. In particular, the slot die coating and ink jet printing processes show great promise for the large-scale manufacturing of MO_X ETLs. However, the solution processing method is still widely employed for various MO_X ETLs, particularly processed at low temperatures for efficient planar PSC due to superior crystallinity and fewer defects in the as-deposited films [84]. It must be underlined that the annealing temperature and relative humidity are important factors in the production of good-quality MO_X layers via the process of thermal decomposition [38, 50].

Atomic Layer Deposition (ALD) Method

Compact, homogenous, and conformal thin films have been developed by the semiconductor industry through the use of the ALD technique, a critical technology for precisely controlling film growth [85]. The film thickness may be easily controlled, and it even allows for the formation of films on textured substrates. The thickness of the MO_X ETL plays an important role in the actual performance resulting in the device. An adequate thickness is sufficient to provide enough electron transport as well as to not lose its transparent characteristic. A very thin layer may lead to reduced coverage with more recombination whereas a very thick layer may restrict the movement of electrons. Also, an optimal thickness of about 30-50 nm of SnO_2 ETL has been shown in studies to give the best performance in planar perovskite solar cells. Typically, an ALD cycle contains the following four steps: The first step involves exposing the first precursor to deposit

a film on the substrate within the reactor chamber; the second step involves the purging or removal of additional first precursor and byproducts; the third step involves exposing the second precursor; and the fourth step purge or evacuation of the excess second precursor and byproducts. Figure 3b depicts the deposition of ZnO via the ALD technique [37, 86]. ALD deposition is advantageous for flexible substrates since it allows the development of very crystalline layers at low growth temperatures. So far, ALD has shown to be an effective technique for producing low-temperature treated MO_X ETLs for high-grade PSC primarily including TiO_2 [87], ZnO[88], and SnO_2[89] ETLs. However, large-scale production by the ALD technique might not be suitable due to its cost, duration, and reliance on the purity of the substrates.

Chemical Bath Deposition (CBD) Method

CBD is another well-established method for depositing semiconductor metal oxide layers by submerging the substrates in diluted solutions of metal ions as well as OH^- or S^{2-} ion sources as displayed in Figure 3c [90]. The CBD technique has proven to be ideal for the development of semiconductor layers particularly for Cu(In, Ga)Se_2 and Cu_2ZnSnS_4 solar cells, like Cadmium sulfide, zinc oxide, or zinc sulfide [91, 92]. Particularly, recent studies have revealed that the CBD approach can be used to produce incredibly efficient MO_X ETLs for PSC such as titanium dioxide, zinc oxide, tin oxide, and iron oxide with definite arrangement [93, 94]. Low fabrication costs, simple growth adaptability, and excellent reproducibility are advantages of the CBD approach, which is beneficial in large-scale processing at low temperatures [38] However, the temperature, concentration, and P_H value during growth have a significant impact on the formation of thin layers.

Other Deposition Methods

There are other efficient ways available to develop MO_X ETLs processed at low temperatures in accordance with various physicochemical features of substances in addition to the deposition processes discussed before.

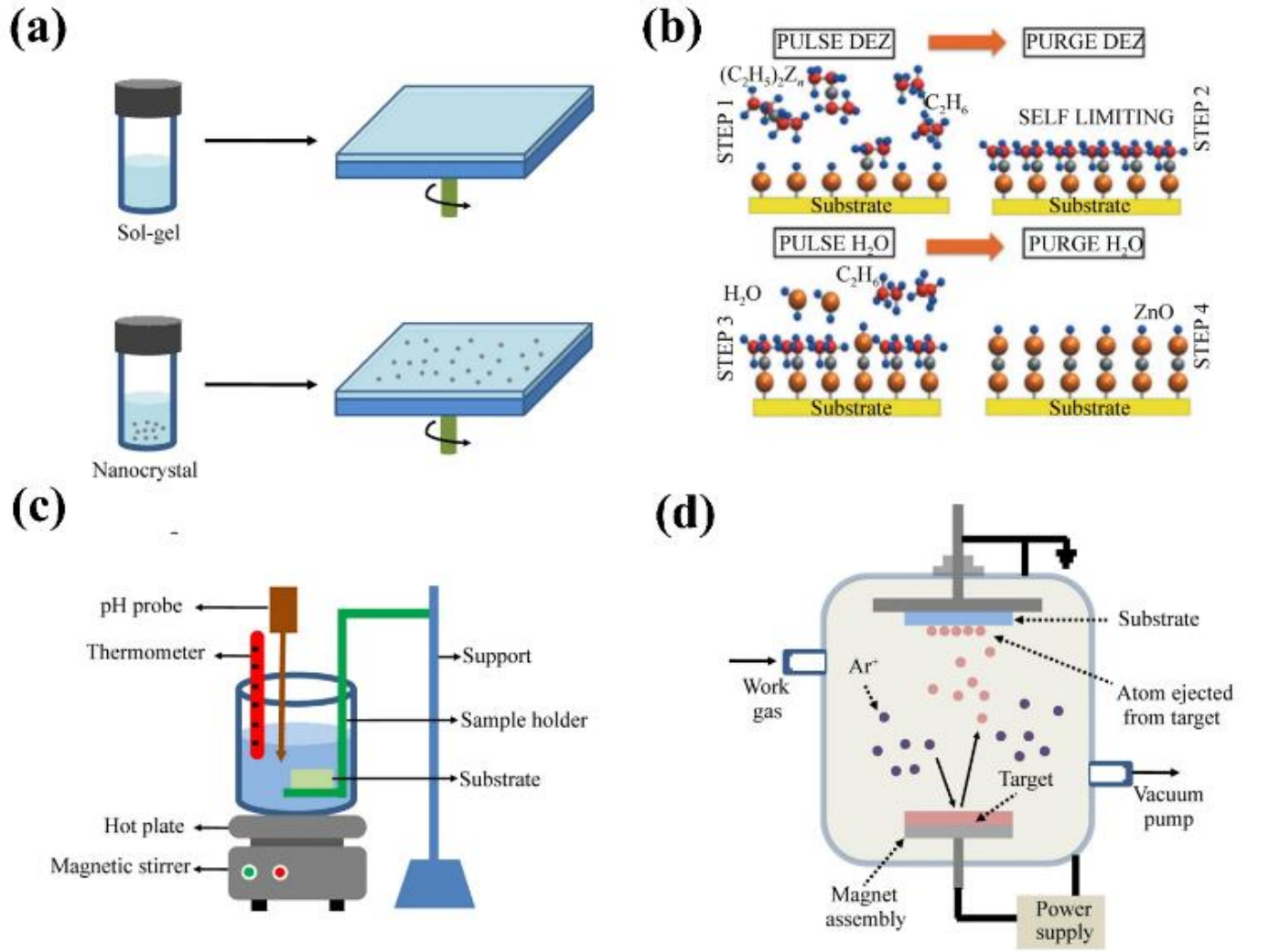

Figure 3. Diagrammatic illustration of the common MO_X ETL deposition techniques: (a) solution process; (b) ALD for ZnO layer; (c) CBD; and (d) magnetron sputtering | adapted from Ref. [95].

For instance, electrochemical deposition (ED) is another significant technique for producing high-quality MO_X thin films and has previously been used to develop TiO_2, ZnO, and SnO_2 ETLs in conventional PSC [96-98]. The advantages of a facile, quick deposition and low-temperature preparation are exhibited by the ED approach. Additionally, by controlling the current density and deposition duration, it is possible to accurately regulate the thin film's properties after deposition with a firm connection to the substrate [50]. Other physical deposition methods used for the deposition of MO_X ETLs include magnetron sputtering displayed in Figure 3d and electron beam evaporation [99, 100]. These methods offer good potential for producing flexible electronics because MO_X can crystallize simultaneously with substrate deposition, effectively avoiding post-annealing. The drawbacks of electrochemical deposition and magnetron sputtering in depositing ETLs for PSCs include limited material choice, uniformity issues, and process complexity [101-103].

The main factors influencing the growth of MOX ETL are substrate preparation, deposition parameters, and target material characteristics. It's also crucial to apply post-deposition treatments and get the appropriate film thickness. Moreover, charge transport and device stability can be strongly impacted by interface engineering at the intersections of ETLs and adjacent layers.

Different MO_X used as an ETL Material in PSC

Titanium Oxide (TiO_2) Based ETL in PSC

TiO_2 thin layers annealed at low temperatures have been frequently created using the solution-processed approach. TiO_2 nanoparticles (NPs) with good dispersion are typically favored for direct deposition on conductive substrates in planar PSC. An inverted PSC using a flat TiO_X film as ETL was first successfully fabricated by Snaith et al. [22]. The PSC treated at all low temperatures yielded a champion PCE of over 6% on flexible polymer substrates. Then, using a nonaqueous technique, they employed $TiCl_4$ to synthesize TiO_2 NPs. This resulted in a high-quality thin film of TiO_2 devoid of cracks, as seen by the SEM picture in Figure 4a-b. [104]. The conductivity of the TiO_2 film was greatly enhanced when titanium di-isopropoxide-bis was added, improving PCE up to 15.9% and proving the viability of processing at low temperatures in conventional PSC. Conings et al. proposed a low-temperature solution processing route for titanium dioxide ETL synthesized by facile one-pot fabrication NPs dispersion for regular PSC [105]. The TiO_2 layer is also suitable for roll-to-roll fabrication on foils made of plastic since it just needs a heat treatment at 135 °C. To modify carrier behavior and boost conductivity, Zhou et al. deposited ETL at low temperature (150 °C) through yttrium (Y) doping into TiO_2 nanocrystals [23]. The use of PEIE and Y-doped TiO_2 lowered the Schottky limit at the ITO/TiO_2 contact. The device performance was significantly increased to 19.3% due to improved transport and extraction of electrons.

Recently, Tan et al. observed that imperfect interfaces and charge recombination between perovskite and TiO_2 interface may effect the PCE and stability of the PSC devices at low temperatures. As an alternative, they strengthened the TiO_2/perovskite interface by adding chlorine (Cl) to the TiO_2 colloidal dispersion. This lowered the density of interfacial traps resulting in superior stability and a PCE of over 20 % via interface passivation. XRD patterns of perovskite layers on TiO_2-Cl and titanium dioxide are illustrated in Figure 4c [106]. As expected from the stoichiometric ratio of the precursors, XRD spectra show no obvious PbI_2 nor other non-perovskite phases in films. It shows a smooth crystalline structure. Recently, Zhao et al. enhanced the quality of a perovskite thin layer by growing it over a low-temperature processed Cl-added TiO_2 ETL. The successful deposition technique involving the addition of cesium chloride to the lead iodide solution resulted in the production of a high-quality perovskite layer. The champion device exhibited a superior PCE exceeding 22%, proving the effectiveness of TiO_2 NPs as ETL and thus a viable option for PSC as in Figure 4d-f [107].

Several additional techniques were also employed to prepare TiO_2 ETLs at low temperatures. An annealing-free titanium dioxide compact layer was originally employed using the ALD approach by Kim et al. for flexible planar PSC [85]. A 20 nm thick TiO_2 compact layer was formed on the plastic conductive substrate less than 80 °C due to plasma accelerated ALD. They showed a very flexible PSC with a 1 mm bending radius, whereas 10 mm bending radius devices were able to sustain 1000 cycles while retaining 95% of their original PCE. Furthermore, Yella et al. tailored a nanocrystalline TiO_2 layer at low temperatures via the CBD approach in PSC and achieved a reasonable PCE of 13.7 %. [109]. Due to the larger interfacial area compared to planar anatase TiO_2, the resultant rutile titanium dioxide was more efficient in extracting electrons from the perovskite layer. Mg-doped rutile TiO_2 ETL treated at low temperature (70 °C) was also prepared by Liao et al. using the CBD approach, together with the carbon as an anode in PSC [110]. The optimal device exhibited a remarkable PCE of 15.73 %. Magnetron sputtering is a further intriguing method for titanium dioxide ETL deposition. Chen et al. deposited TiO_2 ETL over a conductive substrate using low-temperature radio frequency (RF) magnetron sputtering By using this technique, the thickness of the TiO_2 layer could be modified to create a flexible PSC with a PCE of 8.9 % [111]. A planar flexible PSC sputtering process was further investigated by Yang et al [99]. A thick amorphous titanium dioxide ETL treated at low temperatures facilitated increased electron extraction from the layer of perovskite and enhanced electron movement, enabling the fabrication of a flexible device with a 15.07 % PCE. A recent optimization technique for RF magnetron sputtering encouraged the the enhancement in PCE of PSC to roughly 16% by utilizing flexible substrates with small, and uniform TiO_2 nanoparticles-based ETL [112]. The device architecture must be optimized to achieve optimum performance in perovskite solar cells with MOX ETLs.

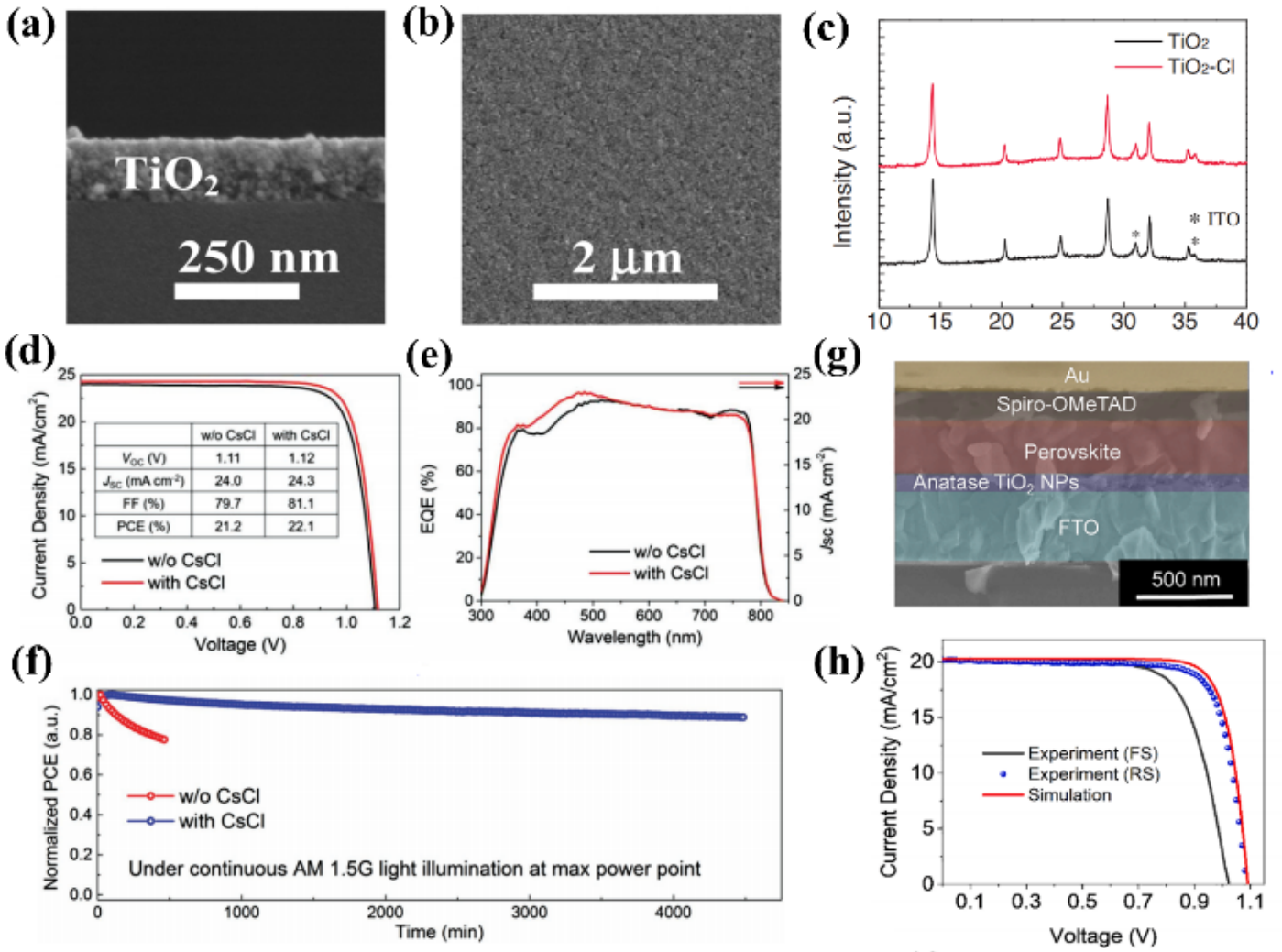

Figure 4. (a) SEM cross-sectional image of glass coated with 3.54 (w/%) TiO_2 NPs with a thickness of 100–120 nm; (b) Top-view SEM image of low-temperature TiO_2 |adapted from Ref. [104]; (c) XRD patterns of perovskite layer deposited atop TiO_2 and TiO_2-Cl ETLs |adapted from Ref. [106]; (d) J–V characteristic curves are shown for the reverse scans (from 1.15 to −0.01 V) with (red) and without CsCl (black); (e) EQE spectra of the same; (f) Testing the PSC's long-term stability without CsCl (red) and with CsCl (blue) at MPP under constant AM 1.5G illumination |adapted from Ref. [107]; (g) SEM cross-sectional image of PSC using the low temperature processed titanium dioxide ETL; and (h) Comparison of the J-V parameters for the top-performing planar PSCs between simulations and experiments (forward scan (FS) and reverse scan (RS)) |adapted from Ref. [108]

For example, the use of buffer layers, optimization of ETL thickness, and engineering an interface can vastly improve charge extraction and dramatically reduce recombination. This includes using a thin interfacial layer between the perovskite and MOX ETL to promote level alignment in energy and defect passivation, resulting in enhancements in PCEs. Furthermore, the devices exhibited steady power output (SPO) up to two hundred cycles of bending, showing the efficacy of the sputtering method. Shahiduzzaman et al. reported further development in treating TiO_2 ETL at low temperatures to produce high-performing PSCs that are suitable for flexible substrates [113]. The optimized ETL was prepared by spin-coating single-phase crystalline anatase titanium dioxide nanoparticles with a median diameter of 6 to 10 nm. In comparison, the most efficient superstrate configuration of a planar device has a PCE of 17.1 % and a J_{SC} of 20.3 mA/cm^2 as shown in Figure 4g-h. Lee et al. use a low-temperature processed bilayer of SnO_2/TiO_2 as an ETL and achieve a PCE of 15.36% [114]. The deterioration of SnO_2 can be stopped and the interfacial contacts between the light-absorbing layer and the ETL may be increased by using low-temperature-processed mesoporous TiO_2. The power conversion efficiency of SnO_2/TiO_2 bilayer-based PSCs was much greater than that of single SnO_2 ETL-based PSCs. Nam et al. produced mesoporous-structured TiO_2-based PSCs with outstanding photovoltaic performance at low temperatures for the first time by demonstrating a successive surface engineering technique using oxygen plasma treatment [115]. The low-temperature solution-processed TiO_2 layer's organic additives were effectively eliminated by the oxygen plasma treatment. Increases in $MAPbI_3$ particle size and infiltration depth into the mesoporous-structured TiO_2 layer were brought

about by the oxygen plasma treatment's enhanced wettability of TiO_2 layers. Furthermore, the PCE of 14.82% was attained by reducing the oxygen vacancies in the TiO_2 layer, which served as trap sites, using an oxygen plasma treatment.

Zinc Oxide (ZnO) Based ETL in PSC

ZnO NPs solutions offer certain unique characteristics; such as a straightforward and controllable synthesis route and the ability to fabricate thin layers processed at low temperatures. These unique features have been thoroughly investigated for the utilization of ZnO as ETL in PSC. Liu and Kelly initially introduced ZnO NPs-based ETL in PSC in 2014 [32]. The compact pinhole-free ETL of ZnO NPs was prepared by employing a solution-processed approach by mixing KOH and $Zn(CH_3COO)_2.2H_2O$ dispersions and further low-temperature post-annealing treatment. The high crystallinity of ZnO NPs exterminated the need for high-temperature post-treatment. The perovskite layer deposited atop ZnO ETL exhibited large grain sizes with visible grain boundaries and the corresponding devices showed PCE of 10.2 % and 15.7 %, for flexible and rigid substrates, respectively.

Hwang et al. stated a complete slot die-coated PSC assembled of ZnO NPs ETL using a handmade 3D printer under ambient conditions. [116]. The optimized PCE of 11.96 % provided the way forward for low-cost and bulk manufacturing of PSC. In the meanwhile, a ZnO/perovskite/carbon planar structure PSC with a metal-electrode-free design and HTL was reported by Zhou et al. Moreover, flexible devices' mechanical strength can be greatly increased by employing this special structure [117]. Song et al. applied industrial ZnO NPs to produce ETL at low temperatures for PSC using a spin coating technique and used di-amino methyl carbonium ion instead of methylamine to produce the absorber material by consecutive layering approach to overcome the problem of thermal instability in ZnO-based PSC as illustrated in Figure 5a-d [118].

The perovskite layer's thermal stability deposited atop zinc oxide ETLwas significantly increased with formamidinium lead iodide due to the fundamental resilient character of formamidinium contrasted to methylammonium in methylammonium lead iodide, and the ZnO-$FAPbI_3$ planar structures exhibited PCE of 16.1% after optimization. $FAPbI_3$ was further substituted with triple-cation perovskite, the PSC achieved a higher PCE of 18.9 % with superior environmental photostability and durability [119]. Additionally, when $FAPbI_3$ was replaced with triple cation perovskite, the same ZnO NPs-based ETL might be used to develop a steady absorber of light using a single-stage deposition technique. A highly transparent ZnO NPs solution was prepared recently using an ultrasonic-assisted approach, which made it possible to prepare a denser and more homogeneous ZnO layer. In addition, a room-temperature aging stage of ZnO thin film was also investigated in this work to enhance the thermal resistance between ZnO and $MAPbI_3$ interface. High-quality ZnO and perovskite thin films contributed synergistically to prevent device degradation, showing good stability even after being exposed to air after 45 days. The SEM images and JV curves are shown in Figure 5e-h [120].

Yang et al. described a method to synthesize ZnO ETL at low temperatures and treated it with an aqueous solution approach employing $[Zn(NH_3)_x](OH)_2$, a solution containing an ammine-hydroxo zinc combination [121]. Consequently, a device with an enhanced V_{OC} of 1.07 V was developed by lowering the ZnO layer annealing temperature to 150 °C. The ZnO NPs atop the perovskite layer allowed inverted PSC to acquire both inorganic charge transport layers (ETL and HTL) and significantly increased device stability with a stabilized PCE of 16.1 % [118]. Similar to this, Savva et al. used aluminum-doped ZnO (AZO) ETL in an inverted PSC [122]. The characteristics of AZO as MO_X ETL can be further optimized by adjusting energy levels to recognize charge carrier transport, and eliminating the pinholes resulting in an enhanced PCE, improved durability, and stability of PSC.

In a quest to find alternative deposition techniques, Lee et al. used the ALD technique to prepare compact ZnO ETL at 80 °C for planar PSC following the comprehensive analysis of film thickness and morphology [123]. Yuan et al. achieved a PCE of 13.1% using this technique [88]. They revealed that the precursor utilized for the formation of a compact ZnO layer using ALD kept at ambient temperature might assist in the formation of $CH_3NH_3PbI_3$. To further develop low-temperature and solution-processed, flexible PSCs, Mathews et al. utilized ZnO nanorods to develop a compact ETL for PSC using the CBD and ED techniques [94]. Zhang and Pauportè used the ED technique to deposit ZnO ETL processed at low temperatures [97]. They observed and compared how the "one-step" and "two-step" techniques for making $CH_3NH_3PbI_3$ were affected by the ZnO and TiO_2 ETLs. The outcomes showed that an ideal device efficiency of 15% might be obtained via combining a perovskite film made by a "one-step" method with a little overvoltage electrodeposited ZnO layer. The impact of RF magnetron sputtering settings on the formation of zinc oxide ETL quality was investigated by Tseng et al. [124]. They discovered that the electrical and electronic characteristics of zinc oxide film were significantly influenced by O_2 voids, it could be managed by altering the ratio of argon to oxygen used as working gases during sputtering. Sputtering was found to be the optimal way to develop ZnO ETLs with reasonable characteristics, and a PCE of 15.9 % was achieved under the Ar environment. Additionally, they used an analogous approach to develop a high-quality film of Al-doped ZnO on an ITO substrate with complete coverage. This layer showed improved band alignment with methylammonium lead iodide, better conductivity, and superior acid resistance than zinc oxide [125].

Consequently, the performance of the PSC using the modified ETL was significantly enhanced. Lai et al. used a C-60 interlayer acting as a protective layer between the sputtered ZnO and perovskite to prevent sputtering damage to the absorber layer and contributed to better device performance [126]. Similarly, Liu et al. modified the CH_3NH_3Cl to increase the stability of ZnO-based PSC [127].

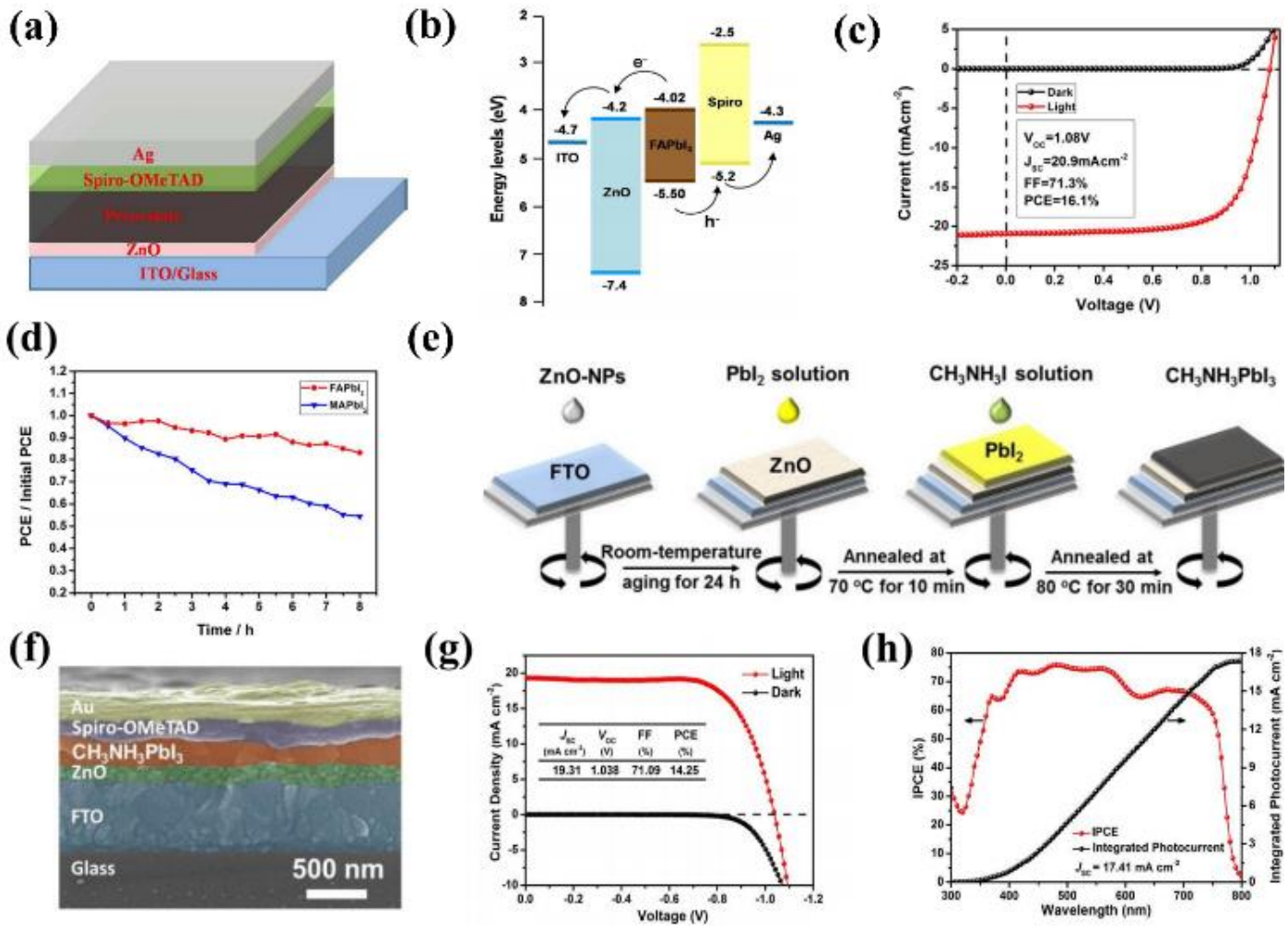

Figure 5. (a) Schematic diagram of ITO/ZnO/$FAPbI_3$/spiro-OMeTAD/Ag PSC; (b) Energy level diagram of the same; (c) Light (red line) and dark (black line) J-V curves (black line); (d) Photostability of $FAPbI_3$ and $MAPbI_3$ absorber material based PSC|adapted from Ref. [118]; (e) Diagrammatic representation of the steps involved in preparing a stable ZnO/$MAPbI_3$ interface by combining a two-stage sequential spin coating technique for the methylammonium lead iodide layer with an aging step for the ZnO layer; (f) SEM cross-sectional image of a complete PSC using zinc oxide ETL; (g) For the ideal zinc oxide based PSC device, the JV curve was evaluated in the dark (black line) and under 100 mW cm^{-2} AM 1.5G illumination (red line); and (h) EQE spectrum of the same |adapted from Ref. [120].

The PSC was fabricated with the configuration ITO/ZnO–MACl/$MAPbI_3$/Spiro-OMeTAD/MoO_3/Ag. The MACl-modified devices exhibited superior photovoltaic parameters (JSC of 21.96 mA/cm^2, VOC of 1.10 V, FF of 77.1 %, and PCE of18.7%) relative to unmodified pristine ZnO-based devices (PCE of 16.55 %).

Tin Oxide (SnO_2) Based ETL in PSC

SnO_2, a naturally occurring, nontoxic, inherently n-type semiconductor with unique characteristics such as excellent stability, superior electron mobility, and high transparency, holds enormous potential as an ETL material in PSC. Tin-based precursors like tin chloride, tin tetrachloride, or hydrates like tin chloride dihydrate and tin chloride pentahydrate are frequently utilized to produce tin oxide thin layers in the sol-gel method. Ke et al. used a precursor of $SnCl_2{\cdot}2H_2O$ to develop SnO_2 thin films through thermal annealing in ambient for one hour at 180 °C in 2015 [82]. After a 15-minute UV-ozone treatment, it became feasible to deposit the perovskite layer atop tin oxide ETL and the champion device showed a PCE of 17.21 %. Zuo et al. used a similar technique for creating a SnO_2 ETL-based perovskite solar cell with an exceptional PCE of 20.23% after upgrading perovskite with a polymer template as displayed in Figure 6a-c [128]. Dong et al. suggested an alternate sol-gel technique by refluxing atmospheric oxygen and water (reflux condensation technique), which considerably accelerated the decomposition and oxidation of $SnCl_2{\cdot}2H_2O$ precursor in an ethanol-based solution and reduced the thermal decomposition temperature as shown in Figure 6d. SnO_2 precursor solution might be cooled below 80 °C as a result.

On both flexible and stiff substrates, the regular planar PSC devices utilized this SnO_2 as ETL and achieved PCE of 19.2% and 16.11%, respectively [129]. Subbiah et al. activated the precursor layer at ambient temperature using a low-power nitrogen RF Plasma. The strong ultraviolet photons from the nitrogen plasma broke -OR and -OH groups, which aided in the creation of the MO_X metal framework. The PSC relying on nitrogen plasma processed tin oxide ETL manifested a PCE of 20.3 % on stiff substrates. On PET substrates, a flexible PSC was also fabricated using the aforementioned technique. The PSC exhibited an outstanding PCE of 18.1 % by retaining 90 % of its original PCE even after a thousand hours as illustrated in Figure 6e [130]. In contrast, the high-temperature annealing is avoidable since the SnO_2 NPs are prepared prior to deposition. Song et al. dispersed industrial-grade tin oxide nano particles (approximately 22 to 43 nm) in C_4H_9OH to develop a thin compact ETL via spin-coating at temperatures in PSC [81]. However, the SnO_2 NPs exhibited irregular morphology with random size distribution of nanoparticles resulting in a low device efficiency of 13 %.

Additionally, You et al. utilized commercial tin oxide NPs colloidal solution to synthesize a pinhole-free compact ETL with a uniform particle size of 3 to 4 nm processed at low temperatures as shown in Figure 6f,g [131]. Using a PbI_2 passivation, a certified efficiency of device 19.9 % was attained in PSC. By further adjusting lead iodide contents, perovskite solar cells subsequently showed efficiencies of 21.6 % for small-size devices (0.0737 cm^2) and 20.1 % in large sizes (1 cm^2), with a certified PCE of 20.9 % for small-size devices [132]. In 2019, the same group reported less non-radiative recombination in PSC by reducing the interfacial defects, and higher efficiency PSC was fabricated due to the passivation of surface imperfections/defects using PEAI. The optimal devices exhibited a higher V_{OC} of 1.18 V with a certified PCE of 23.32 % [133]. A slot die approach for printing good quality tin oxide layers for effective flexible PSC was developed by Bu et al. to examine the solution printability of tin oxide nano particles on plastic substrates [134]. The interfacial contacts were passivated using a general potassium passivation approach to reduce the inherent hysteresis developed by SnO_2 ETL-based PSC. The performance of the small-size flexible PSC was 17.18 %, and the efficiency of the large-size (5 cm to 6cm) flexible modules was over 15 % with no hysteresis.

In addition to commercial SnO_2 colloidal NPs, Yang et al. synthesized SnO_2 quantum dots by mixing thiourea and $SnCl_2{\cdot}2H_2O$ to produce excellent quality tin oxide quantum dots with variable carrier concentrations. A highly stable PCE of 20.32 % with FTO glass substrates and 16.97 % on flexible PEN substrates was obtained for conventional PSC [135]. Similar to TiO_2 and ZnO, SnO_2 thin films can be prepared via the ALD technique. Baena et al. employed ALD to develop compact tin oxide thin layers, which displayed an optimistic and balanced energy level with the perovskite layer [136]. The PSC demonstrated a behavior free of hysteresis with a remarkable PCE of 18 % and a very high V_{OC} of 1.19 V. Wang et al. used plasma-enhanced atomic layer deposition (PE-ALD) to reduce the temperature of deposition (<100°C) to enable low-temperature industrial production of PSC [137]. On flexible substrates and glass, tin oxide ETL-based devices showed PCE of 19.03 % and 16.80 %, respectively, revealing the potential of this low-temperature deposition method. Additionally, they induced the formation of the SnO2 layer by introducing water vapor, potentially facilitating a more comprehensive reaction of the organic precursor and resulting in the production of highly purified tin oxide. A notable PCE of 18.36% was achieved by the flexible PSC based on the obtained SnO_2 [138]. SnO_2 films were also prepared using the CBD technique. A straightforward approach combining SC and CBD to produce SnO_2 ETL was disclosed by Anaraki et al. [139]. They spin-coated a SnO_2 seed layer first, and as a post-treatment on the spin-coated films, they grew a SnO_2 layer using the CBD approach. The SC-CBD approach for depositing the SnO_2 layer showed effective hole-blocking abilities and increased repeatability. The resulting PSC has a high V_{OC} of 1.214 V and an efficiency of 20.7 % under maximum power point tracking. Bu et al. further used the CBD approach [140]. A small-size perovskite solar cell (6x6 cm) sub-module was combined with a unique quadruple-cation perovskite to produce PCEs of 20.56 % and 15.76 %, respectively.

In addition, several new deposition methods have emerged, including electrochemical deposition [98], combustion [141], pulsed laser deposition [142], and E-beam evaporation [100]. E-beam evaporation stands out among them as a viable option since it allows for the simultaneous production of hundreds of SnO_2 ETL substrates, which justifies industrial use. Fang et al. demonstrated the effective SnO_2 ETL-based planar perovskite solar cell using this deposition method with the highest PCE of 18.2 % without any interface modification [100]. Kim et al.examined the impact of K treatment on the tin oxide electron transport layer. It was noticed that the use of KCl treatment boosted the CBM at the perovskite/SnO_2 interface by raising the Fermi level and conduction band maximum energy of tin oxide and narrowing the band gap of the perovskite absorber through K^+ diffusion. J-V hysteresis was nearly diminished due to improvements in the alignment of the band and passivation of defects achieved by the potassium chloride treatment [143]. Huang et al. reported on the low-temperature UV curing procedure used to make SnO_2 films and their use as the electron-transporting layer in planar PSCs [144]. The formation of these SnO_2 ETLs involves subjecting the as-deposited precursor films to UV irradiation at a very low temperature (70 °C) without any additional thermal or chemical treatment. Using these films acting as ETLs, photovoltaic devices demonstrated the greatest efficiency of 16.21%, significantly greater than those using SnO_2 ETLs made using a traditional thermal annealing method (11.49%). Shekargoftar et al. investigated the preparation of SnO_2 using plasma treatment at a low temperature of 60 °C [127]. A set of SnO_2 films treated by traditional thermal annealing was contrasted with SnO_2 films treated by plasma. Films with homogenous surfaces and a highly crystalline structure were produced by plasma treatment.

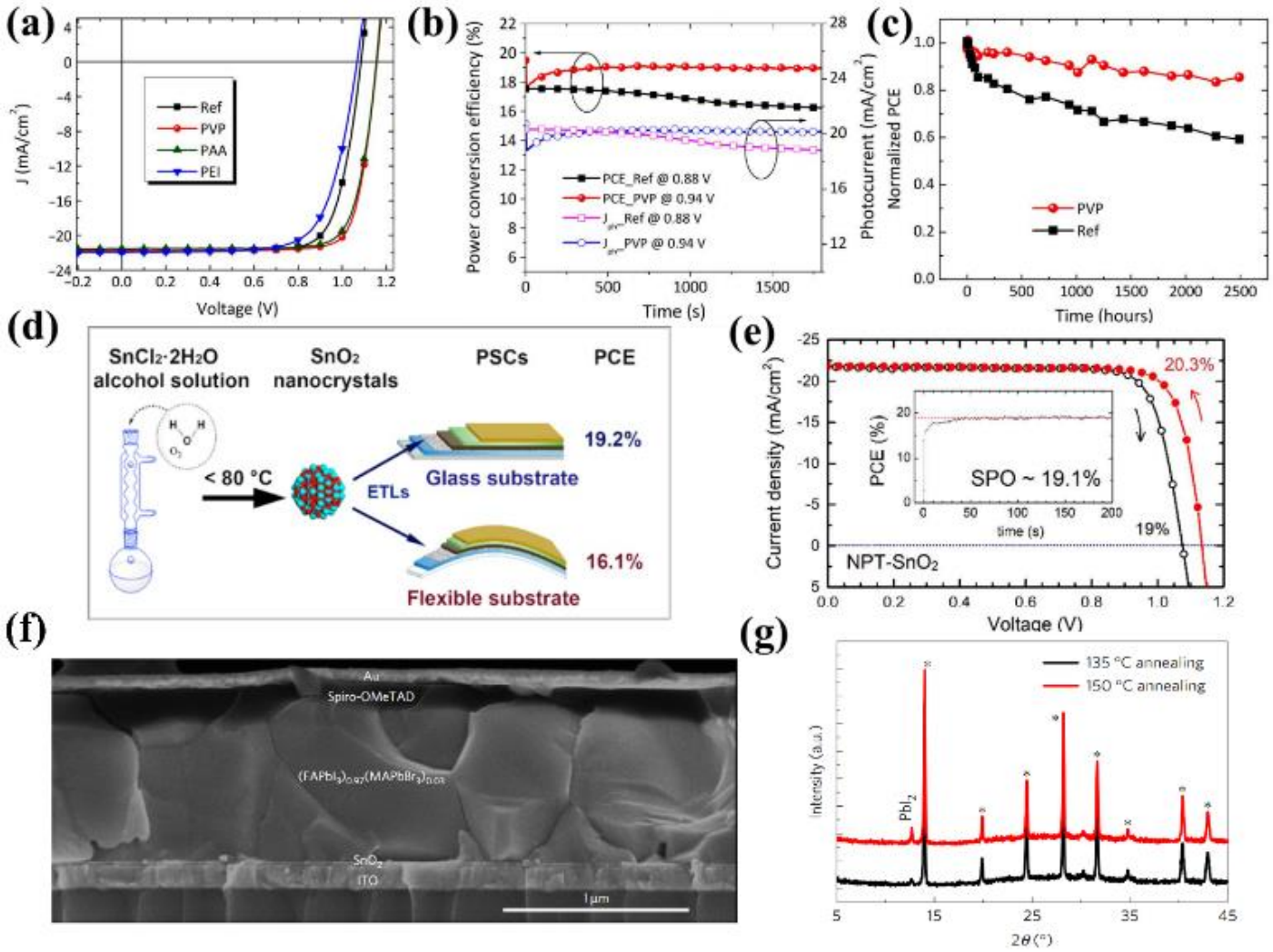

Figure 6. (a) J-V curves; (b) EQE spectra; (c) shelf-life stability with and without PVP treatment of $CH_3NH_3PbI_3$ solar cell devices with various polymers converted from microporous PbI_2 |adapted from Ref. [128]; (d) Novel approach to preparing low-temperature SnO_2 nanocrystals |adapted from Ref. [129]; (e) Planar PSC with light JV curves at 100 mW/cm^2 (1 sun) intensity using TA-SnO_2 and NPT SnO_2 layers as ETL in both FS and RS orientations produced a PCE of 20.3% |adapted from Ref. [130]; (f) SEM cross-sectional image of PSC with configuration glass/ITO/SnO_2/$(FAPbI_3)_{0.97}(MAPbBr_3)_{0.03}$/Spiro-OMeTAD/Au; (g) XRD patterns of perovskite films annealed at 130 °C and 150 °C, respectively |adapted from Ref. [131].

Only very few variations in the charge extraction of the SnO_2 layers produced by heat annealing and plasma were found upon further investigation. The qualities of films created by plasma deposition are quite competitive when compared to films created using thermal annealing. Their findings revealed that the efficiency of this plasma treatment reached 15.17%, a value comparable to the efficiency achieved through thermal annealing, which stood at 15.91% for SnO_2.

Iron Oxide (α-Fe_2O_3) Based ETL in PSC

Hematite (α-Fe_2O_3) is a thermodynamically stable n-type semiconducting iron oxide that has attracted attention due to its low UV photocatalytic activity, which is useful for prolonging the UV stability of PSCs [53]. The crystal structure and light absorption profile of hematite are shown in Figure 7a. α-Fe_2O_3 has an optical band gap of 2-2.3 eV and is a cheap, abundant, and non-toxic material [145-147]. Since α-Fe_2O_3 has a lower conduction band minimum (CBM) than TiO_2, it facilitates the process of extracting electrons from the perovskite layer [148]. Hu et al. utilized α-Fe_2O_3 as the charge transfer layer (CTL) in $MAPbI_3$ PSC, exhibiting 11 % PCE and enhanced stability in comparison to a TiO_2-based PSC. In the α-Fe_2O_3 ETL-based PSC, the significant potential across the perovskite film promoted better extraction of charges and less accumulation of charges at the interface [66, 149]. Guo et al. utilized nickel-doped α-Fe_2O_3 ETL in planar heterojunction PSC. The dopant addition might increase electronic conductivity and cause a reduction in the injection of electrons and transfer from the perovskite conduction band..

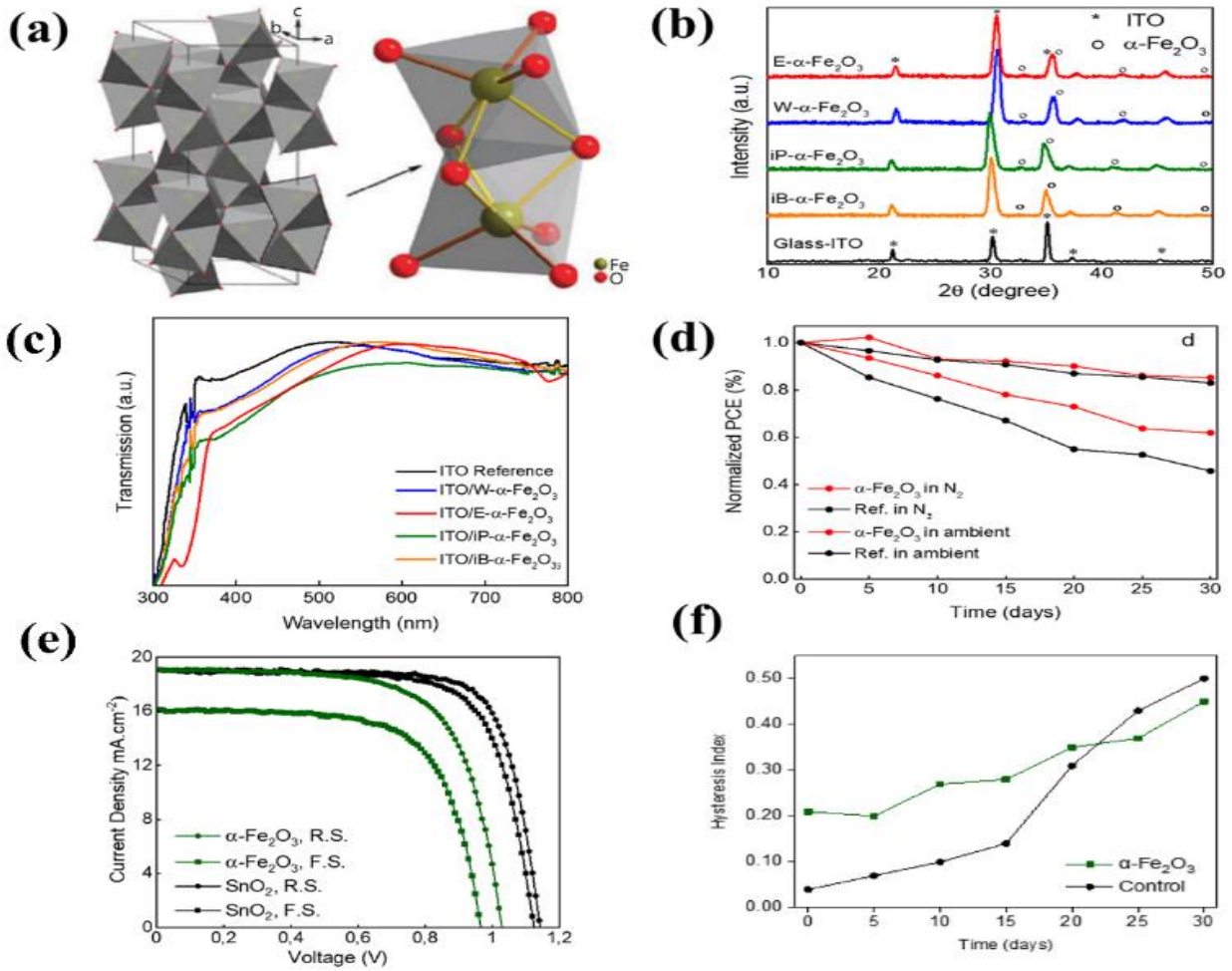

Figure 7. (a) Crystal Structure of α-Fe_2O_3; (b) XRD patterns α-Fe_2O_3 films deposited atop ITO using different solvents (deionized water, ethanol, isopropanol, and isobutanol) |adapted from Ref. [110]; (c) Transmission spectra of ITO/α-Fe_2O_3 thin layera with various solvents; (d) shelf-life stability conducted using identical conditions for the control and champion devices |adapted from Ref. [153]; (e) J-V curves at 10 mg/mL concentration of hematite EEL and a SnO_2 EEL control device; and (f) Champion and control device hysteresis index |adapted from Ref. [154].

Due to this, the device became substantially less responsive to direction and rate of scanning, or reduced hysteresis, due to a high reduction in the charge buildup at the perovskite/ETL interface. The optimized PSC shows a 14.2 % competitive PCE with a high Jsc of 22.35 mA/cm^2, Voc of 0.92V, and FF of 69.1% when scanned in reverse under standard AM-1.5 sunlight illumination. In addition, it is possible to obtain good stability for devices exposed to high UV radiation levels and ambient air [150]. Hou et al. used an α-Fe_2O_3 fullerene bilayer in a planar PSC and demonstrated a PCE of 14 % (2-38.) With a low trap density and strong electron mobility, Zhu et al. were able to construct Ti−Fe_2O_3 ETLs with a PCE of 17.8 % and better charge transfer [151]. Guo and colleagues utilized interfacial engineering to develop a bifunctional alteration of the α-Fe_2O_3/perovskite interface through the use of PbI_2. This led to a notable enhancement in the alignment of energy levels and the suppression of JV hysteresis [152]

Qureshi et al. examined the impacts of solvents on the optoelectronic characteristics of α-Fe_2O_3 thin films by working on the solvent-assisted crystallization of ETLs. An n−i−p-configured PSC with an optimized ethanol-based (0.2M) α-Fe_2O_3 ETL demonstrated a decreased hysteresis index of 0.04 and a PCE of 13%, out of the several solvents utilized in their investigation (de-ionized water, C_2H_5OH, iso-propanol, and iso-butanol). They reported that the development of a compact shape of ETLs without pinholes leads to improved charge transfer efficiency, decreased interfacial recombination, and free-of-crack surface coverage of the perovskite layer atop an α-Fe_2O_3 ETL as shown in Figure 7b-d [153]. To prepare low-temperature solution-processed hematite ETLs, Qureshi et al. used natural α-Fe_2O_3 as an ETL. The completed device manufacturing was done at a temperature lower than 150 °C to demonstrate the cost-effectiveness of this innovative electron extraction layer (EEL). The optimal concentration-based device showed a PCE of 13.3 % and a V_{OC} of 1.03 V with long-term shelf life stability. The enhanced photovoltaic properties are due to the smooth surface structure of CsFAMA atop natural α-Fe_2O_3 EEL, high crystallinity of natural α-Fe_2O_3, and lower interfacial recombination as in Figure 7e-f [154].

Other Metal Oxide ETL Based in PSC

It is possible to look at other binary MO_X that are less renowned as compared to TiO_2, SnO_2, ZnO, and α-Fe_2O_3 ETL materials. Dong et al. prepared a chromium oxide (Cr_2O_3) layer on an FTO glass substrate with SC chromium oxide ink without post-annealing [61]. The chromium oxide layer demonstrated great optical transmittance and effective electron transport. A PCE of 16.23% was attained by the planar PSC based on Cr_2O_3 ETL. Similarly, Wang et al. produced cerium oxide (CeO_X) layers at 150 °C employing a basic sol-gel technique [64]. The PCE in PSC was raised to 17.04 % after CeO_X was modified with PCBM, and it displayed greater stability under illumination. Hu et al. employed a solution-processing technique at a low temperature of 100 °C to develop CeO_X ETLs in inverted configuration PSC [155]. The PSC showed an improved PCE of 17.1 % with long-term inert and ambient stability.

Tungsten Oxide (WO_3) is another novel ETL material recently used in PSC with an efficient hole-blocking capability. Wang et al. utilized niobium-modified tungsten oxides ETL modified with plastic substrates at low-temperature [156]. The addition of Nb^{5+} significantly enhanced the PCE up to 15.65 % as shown in Figure 8 a-b. Without any post-treatment, Feng et al. developed Nb_2O_5 ETL by the E-beam evaporated method [59]. Champion PSC devices using rigid and flexible substrates showed PCE values of 18.59 % and 15.56 %, respectively at an optimized thickness of 60-nm Nb_2O_5 layer. Furthermore, the E-beam evaporated niobium oxide is advantageous for flexible PSC in wide areas, and corresponding J_{SC} and V_{OC} values are comparable to those of small-area devices. The primary cause of losses in PCE, which led to a reduced FF, was increased series resistance.

Ternary MO_X differs from binary MO_X owing to their exceptional characteristics qualities including high crystallization and complete surface coverage. Furthermore, the physical & chemical characteristics of ternary MO_X can be enhanced by modifying and tuning their compositions. Shin et al. employed hydrazine to produce Zn_2SnO_4 at a low processing temperature [157]. A PCE of 15.3 % was observed for ternary MO_X ETL-based flexible PSC as shown in Figure 8c-e. Using zinc-stannate nano particles and quantum dots, they also customized the energy levels in the modified electron transport layer. The energy level graded electron transport layer produced by the sequential deposition of nano particles & quantum dots on a flexible substrate demonstrated enhanced electron collection efficiency and boosted power conversion efficiency to 16.5 %. [158].

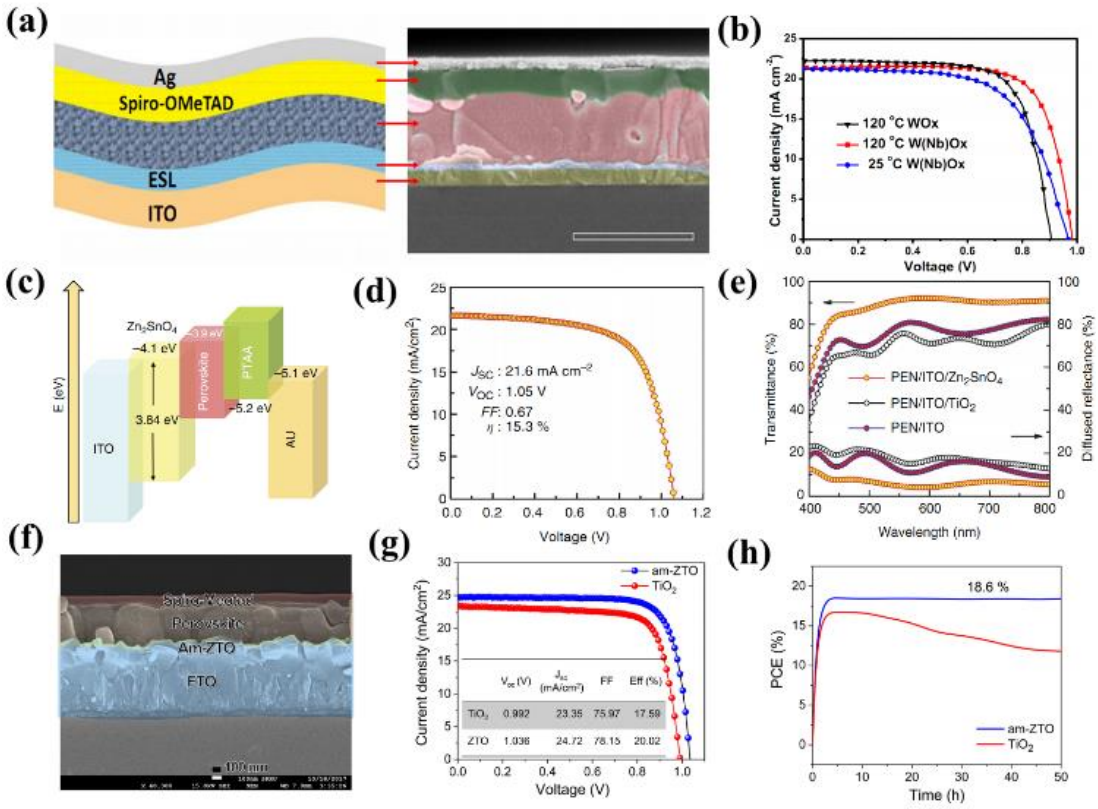

Figure 8. (a) Cross-sectional SEM image displaying each functional layer in the flexible PSC; (b) J-V curves with multiple ESL |adapted from Ref. [156]; (c) PSC energy levels; (d) Under AM 1.5 G illumination, the photocurrent (JV) curve was measured by reverse scanning with 10 mV voltage increment and 40 ms delay intervals; (e) PEN/ITO/ZSO, PEN/ITO/TiO_2, and PEN/ITO substrate transmittance and reflectance spectra |adapted from Ref. [157]; (f) SEM cross-sectional image of PSC with Am-ZTO ETL; (g) JV curves of PSC using am-ZTO ETL and TiO_2 as reference ETL; and (h) MPPT of an Am-ZTO ETL based PSC |adapted from Ref. [159].

Using a sol-gel technique, Jung et al. prepared amorphous Zn_2SnO_4 layers with superior surface homogeneity, fast mobility of electrons, and low-voltage trapping [159]. The resulting perovskite solar cell had better device stability, and negligible hysteresis behavior, and produced a PCE of 20.02 % as shown in Figure 8f-h. $BaSnO_3$ is another semiconducting ternary metal oxide with a large band gap of 3.2 eV. However, large temperature treating of $BaSnO_3$ around 900 °C severely limits its use in flexible devices [160]. Shin et al. produced a colloidal solution of superoxide molecular clusters for the deposition of La-doped $BaSnO_3$ films at temperatures lower than 300 °C [161]. The devices utilizing $BaSnO_3$ ETL in PSC showed superior PCE of 21.2 % and remained at 93% of its initial PCE up to one thousand hours. However, 300 °C is still not a suitable temperature for plastic substrates. To avoid this, Sun et al. manufactured completely dispersed barium stannate nanoparticles via the facile peroxide-precipitate technique and employed them as an ETL in n-i-p configured PSC with low temperature (150 °C) post-treatment. The PSC exhibited a comparative PCE of 10.96 % [72].

The deficiencies of binary MO_X as ETL material were further alleviated by mixing two semiconductors with compensating properties [162]. In comparison to pure WO_X, Wang et al. observed that adding TiO_X to WO_X would increase the Fermi level and reduce interfacial recombination of charge [163]. Consequently, by optimizing the MO_X molar ratios, the PSC achieved a reasonable PCE of 14.47 %. Similarly. Zinc oxide-tin oxide nanocomposite-based thin layers were prepared by Song et al. by simply combining ZnO and SnO_2 NPs [164]. The devices exhibited photovoltaic performance dependent on ZnO/SnO_2 ratio. The planar PSC demonstrated a comparatively high efficiency of 14.3 % with an optimum weight ratio of 2:1. It was noted that the devices with ZnO-SnO_2 ETL realized significant thermal stability compared to bare ZnO ETL-based PSC.

Conclusion and Outlook

The low-temperature solution-treated MO_X are potential applicants as ETLs for effective planar perovskite solar cells, which can drastically decrease the cost of fabrication and be advantageous for flexible and large-module solar cells. In order to comprehend the connection between MO_X ETL and device performance, this review gives an extensive summary of the fundamental characteristics of different MO_X materials, including energy levels, processability, mobility, transparency, and even stability. Then, a brief description of commonly used methods for depositing MO_X ETL was discussed. Finally, a detailed discussion and demonstration of the most recently developed MO_X ETLs in planar PSC with superior performance produced at low temperatures are provided. Single-step processed MOX ETLs at low-temperatures also have some limitations despite the advantages listed above. Uniform film quality and their crystallinity at low temperatures are not easily obtained. The presence of interfacial defects and the possibility for chemical incompatibility with the perovskite layer could be responsible to some extent for poor device performance. For addressing these challenges, surface modifications and doping strategies play a vital role in further improvement. The following critical requirements must be met by an ideal MO_X ETL for best-resulted PSC: (1) outstanding film-forming capabilities via facile and low-cost deposition methods; (2) appropriate energy levels to enable successful charge extraction; (3) fast mobility to facilitate an effective charge transfer; and (4) excellent chemical, optical, and ambient stability for a stable long-term perovskite solar cell.

From this perspective, SnO_2 manifests as an excellent candidate for MO_X-based ETL in regular planar PSC due to its distinctive benefits. Additionally, general methodologies for MO_X optimization such as surface modification, bilayer engineering, composite development, and elemental doping are beneficial in adjusting the MO_X optoelectronic, chemical, and physical characteristics. As a result, it is possible to significantly advance perovskite solar cell technology toward better efficiency and high stability.

Notably, it is an inexpensive and low-energy technique to directly deposit ETLs using nanocrystal solution among the many methods used in producing MO_X ETLs. From this perspective, preparing and using colloidal nanocrystals can be useful in developing the lower-temperature ETLs of a planar perovskite solar cell. These colloidal nanocrystals have outstanding crystallinity and tunable optoelectronic properties. As a result, the ongoing research into innovative MO_X and process optimization for nanocrystal ETL will be a key component in the development of high-efficiency, inexpensive, large-area, and flexible devices. To boost the flexibility of ETL, mixing MO_X with functional organic compounds may therefore be a successful strategy. The organic molecules can strongly adsorb on the MO_X surface, particularly when certain functional groups are interacting with MO_X. Furthermore, by producing an organic network structure, the addition of chemically cross-linked organic elements can change a brittle MO_X ETL using a mechanically robust semiconducting structure. The surface modification of MO_X ETLs may help to increase flexibility by employing this method.

Future Perspectives

Despite significant advancements over the past ten years, further research is still required for low-temperature solution-processed MO_X ETLs. The quest to explore novel electron transport materials with fast mobility, fewer surface imperfections, and suitable alignment of energy bands is an endless process. One of the main constraints impacting the MO_X ETL in flexible PSC is the intrinsically brittle nature of MO_X. Organics; in contrast, exhibit the virtue of good adaptability. The organic modification can also be used to adjust the MO_X surface energy, work function, and wetting characteristics. Owing to the several surface and interfacial cracks in perovskite, various functional groups, including Lewis acid and base, can be added to organic molecules to produce unique linkages with the perovskite layer. These connections can promote interfacial charge transfer, passivate trap states, and reduce the interfacial trap densities, thus improving the performance of the device and lowering hysteresis. All things considered, we believe that through the development and optimization of the MO_X in conjunction

with a thorough understanding of material science, the planar PSC utilizing low-temperature MO_X ETLs has the potential to be a viable commercialization contender in the future due to its significant operational improvements.

References

1. Smalley, R., Future Global Energy Prosperity: The Terawatt Challenge. MRS Bulletin, 2005. 30: p. 412-417.
2. Hoffmann, M., et al., Elemental Applications of Semiconductor Photocatalysis. Chemical Reviews, 1995. 95: p. 69-96.
3. Susanti, D., et al., The Preparation of Dye Sensitized Solar Cell (DSSC) from TiO2 and Tamarillo Extract. Procedia Chemistry, 2014. 9: p. 3–10.
4. Venumbaka, M.R. and D. Rao, Fabrication and performance evaluation of Natural Dye Sensitized Solar Cells Using TiO2 incorporated with Ag nanoparticles. 2017. 4: p. 2325-2327.
5. Isikgor, F.H., et al., Molecular engineering of contact interfaces for high-performance perovskite solar cells. Nature Reviews Materials, 2023. 8(2): p. 89-108.
6. Guo, X., G. Lu, and J. Chen, Graphene-Based Materials for Photoanodes in Dye-Sensitized Solar Cells. Frontiers in Energy Research, 2015. 3.
7. S Lewis, N., Toward Cost-Effective Solar Energy Use. Science (New York, N.Y.), 2007. 315: p. 798-801.
8. Lim, S.P., et al., Enhanced photovoltaic performance of silver@titania plasmonic photoanode in dye-sensitized solar cells. RSC Adv., 2014. 4.
9. O'Regan, B. and M. Graetzel, A low-cost, high-efficiency solar cell based on dye-sensitized colloidal TiO2 films. Nature, 1991. 353: p. 737-740.
10. Gur, I., et al., Air-Stable All-Inorganic Nanocrystal Solar Cells Processed from Solution. Science (New York, N.Y.), 2005. 310: p. 462-5.
11. Li, X., et al., Review and perspective of materials for flexible solar cells. Materials Reports: Energy, 2021. 1(1): p. 100001.
12. Jeon, N.J., et al., Solvent engineering for high-performance inorganic–organic hybrid perovskite solar cells. Nature materials, 2014. 13(9): p. 897-903.
13. Jiang, Q., et al., Interfacial Molecular Doping of Metal Halide Perovskites for Highly Efficient Solar Cells. Advanced Materials, 2020. 32: p. 2001581.
14. Cao, F., L. Bian, and L. Li, Perovskite solar cells with high-efficiency exceeding 25%: A review. Energy Materials and Devices, 2024. 2(1): p. 9370018.
15. Wehrenfennig, C., et al., High Charge Carrier Mobilities and Lifetimes in Organolead Trihalide Perovskites. Advanced materials (Deerfield Beach, Fla.), 2014. 26: p. 1584-9.
16. Lin, Q., et al., Electro-optics of perovskite solar cells. Nature Photonics, 2014. 9.
17. Dong, Q., et al., Electron-hole diffusion lengths > 175 μm in solution-grown CH₃NH₃PbI₃ single crystals. Science, 2015. 347(6225): p. 967-970.
18. Kojima, A., et al., Organometal Halide Perovskites as Visible-Light Sensitizers for Photovoltaic Cells. Journal of the American Chemical Society, 2009. 131(17): p. 6050-6051.
19. Kim, H.-S., et al., Lead Iodide Perovskite Sensitized All-Solid-State Submicron Thin Film Mesoscopic Solar Cell with Efficiency Exceeding 9%. Scientific Reports, 2012. 2(1): p. 591.
20. Li, H., et al., 2D/3D heterojunction engineering at the buried interface towards high-performance inverted methylammonium-free perovskite solar cells. Nature Energy, 2023. 8(9): p. 946-955.
21. Shin, S.S., S.J. Lee, and S.I. Seok, Metal Oxide Charge Transport Layers for Efficient and Stable Perovskite Solar Cells. Advanced Functional Materials, 2019. 29(47): p. 1900455.
22. Docampo, P., et al., Efficient organometal trihalide perovskite planar-heterojunction solar cells on flexible polymer substrates. Nature Communications, 2013. 4(1): p. 2761.
23. Zhou, H., et al., Interface engineering of highly efficient perovskite solar cells. Science, 2014. 345(6196): p. 542-546.
24. Xue, R., et al., Dopant-free hole transporting materials with supramolecular interactions and reverse diffusion for efficient and modular p-i-n perovskite solar cells. Science China Chemistry, 2020. 63(7): p. 987-996.
25. Liu, M., M.B. Johnston, and H.J. Snaith, Efficient planar heterojunction perovskite solar cells by vapour deposition. Nature, 2013. 501(7467): p. 395-398.
26. Iqbal, Z., et al., Interface Modification for Energy Level Alignment and Charge Extraction in CsPbI3 Perovskite Solar Cells. ACS Energy Letters, 2023. 8(10): p. 4304-4314.
27. Xiao, H., et al., Highly Efficient and Air-Stable Inorganic Perovskite Solar Cells Enabled by Polylactic Acid Modification. Advanced Energy Materials, 2023. 13(32): p. 2300738.
28. Ashif, M. and M. Farhana, Promises and Challenges of Perovskite Solar Cells: A Comprehensive Review. BULLET : Jurnal Multidisiplin Ilmu, 2023. 2(5): p. 1147-1157.
29. Wang, J.T.-W., et al., Low-Temperature Processed Electron Collection Layers of Graphene/TiO2 Nanocomposites in Thin Film Perovskite Solar Cells. Nano Letters, 2014. 14(2): p. 724-730.
30. Wojciechowski, K., et al., C60 as an Efficient n-Type Compact Layer in Perovskite Solar Cells. J Phys Chem Lett, 2015. 6(12): p. 2399-405.
31. Kuang, C., et al., Highly efficient electron transport obtained by doping PCBM with graphdiyne in planar-heterojunction perovskite solar cells. Nano Lett, 2015. 15(4): p. 2756-62.
32. Liu, D. and T.L. Kelly, Perovskite solar cells with a planar heterojunction structure prepared using room-temperature solution processing techniques. Nature Photonics, 2014. 8(2): p. 133-138.

33. Jiang, Q., et al., Enhanced electron extraction using SnO2 for high-efficiency planar-structure HC(NH2)2PbI3-based perovskite solar cells. Nature Energy, 2016. 2(1): p. 16177.
34. Singh, T., J. Singh, and T. Miyasaka, Role of Metal Oxide Electron-Transport Layer Modification on the Stability of High Performing Perovskite Solar Cells. ChemSusChem, 2016. 9(18): p. 2559-2566.
35. Haque, M.A., et al., Metal Oxides as Efficient Charge Transporters in Perovskite Solar Cells. Advanced Energy Materials, 2017. 7(20): p. 1602803.
36. Jiang, Q., et al., Towards linking lab and field lifetimes of perovskite solar cells. Nature, 2023. 623(7986): p. 313-318.
37. Zhang, P., et al., Perovskite Solar Cells with ZnO Electron-Transporting Materials. Advanced Materials, 2018. 30(3): p. 1703737.
38. Zhou, Y., X. Li, and H. Lin, To Be Higher and Stronger—Metal Oxide Electron Transport Materials for Perovskite Solar Cells. Small, 2020. 16(15): p. 1902579.
39. Ouyang, D., Z. Huang, and W.C.H. Choy, Solution-Processed Metal Oxide Nanocrystals as Carrier Transport Layers in Organic and Perovskite Solar Cells. Advanced Functional Materials, 2019. 29(1): p. 1804660.
40. Shin, S.S., S.J. Lee, and S.I. Seok, Exploring wide bandgap metal oxides for perovskite solar cells. APL Materials, 2018. 7(2).
41. Niu, G., X. Guo, and L. Wang, Review of Recent Progress in Chemical Stability of Perovskite Solar Cells. J. Mater. Chem. A, 2014. 3.
42. Aung, S.K.K., et al., Reduced hysteresis and enhanced air stability of low-temperature processed carbon-based perovskite solar cells by surface modification. Electrochimica Acta, 2023. 443: p. 141935.
43. Aarik, J., et al., Characterization of titanium dioxide atomic layer growth from titanium ethoxide and water. Thin Solid Films, 2000. 370: p. 163-172.
44. Reyes-Coronado, D., et al., Phase-pure TiO(2) nanoparticles: anatase, brookite and rutile. Nanotechnology, 2008. 19(14): p. 145605.
45. Leijtens, T., et al., Overcoming ultraviolet light instability of sensitized TiO2 with meso-superstructured organometal tri-halide perovskite solar cells. Nature Communications, 2013. 4(1): p. 2885.
46. Xue, S.W., et al., Effects of Post-Thermal Annealing on the Optical Constants of ZnO Thin Film. Journal of Alloys and Compounds, 2008. 448: p. 21-26.
47. Srikant, V. and D.R. Clarke, On the optical band gap of zinc oxide. Journal of Applied Physics, 1998. 83(10): p. 5447-5451.
48. Look, D.C., et al., Electrical properties of bulk ZnO. Solid State Communications, 1998. 105(6): p. 399-401.
49. Yang, J., et al., Origin of the Thermal Instability in CH3NH3PbI3 Thin Films Deposited on ZnO. Chemistry of Materials, 2015. 27: p. 150529083734008.
50. Jiang, Q., X. Zhang, and J. You, SnO2: A Wonderful Electron Transport Layer for Perovskite Solar Cells. Small, 2018. 14(31): p. 1801154.
51. Haghighi, M., et al., Low-Temperature Processing Methods for Tin Oxide as Electron Transporting Layer in Scalable Perovskite Solar Cells. Solar RRL, 2023. 7(10): p. 2201080.
52. Gurudayal, et al., Perovskite–Hematite Tandem Cells for Efficient Overall Solar Driven Water Splitting. Nano Letters, 2015. 15(6): p. 3833-3839.
53. Li, N., et al., Multiple-metal-doped Fe3O4@Fe2O3 nanoparticles with enhanced photocatalytic performance for methyl orange degradation under UV/solar light irradiation. Ceramics International, 2020. 46(11, Part B): p. 19038-19045.
54. Lee, S.-M., et al., Low resistive transparent and flexible ZnO/Ag/ZnO/Ag/WO3 electrode for organic light-emitting diodes. Organic Electronics, 2012. 13: p. 1654–1659.
55. Zheng, H., Y. Tachibana, and K. Kalantar-Zadeh, Dye-sensitized solar cells based on WO3. Langmuir, 2010. 26(24): p. 19148-52.
56. Wang, K., et al., Low-Temperature and Solution-Processed Amorphous WOX as Electron-Selective Layer for Perovskite Solar Cells. The Journal of Physical Chemistry Letters, 2015. 6(5): p. 755-759.
57. Janninck, R.F. and D.H. Whitmore, Electrical Conduction in Nonstoichiometric α-Nb2O5. The Journal of Chemical Physics, 2004. 37(12): p. 2750-2754.
58. Özer, N., D.-G. Chen, and C.M. Lampert, Preparation and properties of spin-coated Nb2O5 films by the sol-gel process for electrochromic applications. Thin Solid Films, 1996. 277(1): p. 162-168.
59. Feng, J., et al., E-beam evaporated Nb2O5 as an effective electron transport layer for large flexible perovskite solar cells. Nano Energy (Print), 2017: p. 1-8.
60. Crawford, J.A. and R.W. Vest, Electrical Conductivity of Single-Crystal Cr2O3. Journal of Applied Physics, 1964. 35: p. 2413-2418.
61. Dong, J., et al., Annealing-Free Cr(2) O(3) Electron-Selective Layer for Efficient Hybrid Perovskite Solar Cells. ChemSusChem, 2018. 11(3): p. 619-628.
62. Julkarnain, M., et al., Optical properties of thermally evaporated Cr2O3 thin films. Canadian Journal on Chemical Engineering & Technology, 2012. 3: p. 81-85.
63. Patsalas, P., L. Sygellou, and S. Kennou, Structure-dependent electronic properties of nanocrystalline cerium oxide films. Physical Review B, 2003. 68.
64. Wang, X., et al., Cerium oxide standing out as an electron transport layer for efficient and stable perovskite solar cells processed at low temperature. Journal of Materials Chemistry A, 2017. 5(4): p. 1706-1712.
65. Hashimoto, T., T. Yamada, and T. Yoko, Third-order nonlinear optical properties of sol–gel derived α-Fe2O3, γ-Fe2O3, and Fe3O4 thin films. Journal of Applied Physics, 1996. 80(6): p. 3184-3190.
66. Hu, W., et al., Hematite electron-transporting layers for environmentally stable planar perovskite solar cells with enhanced energy conversion and lower hysteresis. Journal of Materials Chemistry A, 2017. 5(4): p. 1434-1441.

67. Bohn, C., et al., Effect of Tin Doping on ??-Fe2O3 Photoanodes for Water Splitting. The Journal of Physical Chemistry C, 2012. 116: p. 15290–15296.
68. Young, D., et al., Growth and characterization of radio frequency magnetron sputter-deposited zinc stannate, Zn2SnO4, thin films. Journal of Applied Physics, 2002. 92: p. 310-319.
69. Shin, S.S., et al., High-Performance Flexible Perovskite Solar Cells Exploiting Zn2SnO4 Prepared in Solution below 100 °c. Nature communications, 2015. 6: p. 7410.
70. Cherrad, D., et al., Influence of valence electron concentration on elastic, electronic and optical properties of the alkaline-earth tin oxides A3SnO (A=Ca, Sr and Ba): A comparative study with ASnO3 compounds. Physica B: Condensed Matter, 2011. 406: p. 2714-2722.
71. Galazka, Z., et al., Experimental Hall electron mobility of bulk single crystals of transparent semiconducting oxides. Journal of Materials Research, 2021. 36(23): p. 4746-4755.
72. Sun, R., et al., Ternary oxide BaSnO 3 nanoparticles as an efficient electron-transporting layer for planar perovskite solar cells. Journal of Alloys and Compounds, 2017. 722.
73. Yin, X., et al., Ternary Oxides in the TiO2-ZnO System as Efficient Electron-Transport Layers for Perovskite Solar Cells with Efficiency over 15%. ACS Applied Materials & Interfaces, 2016. 8.
74. Li, X., et al., Rational Design of Solution-Processed Ti-Fe-O Ternary Oxides for Efficient Planar CH(3)NH(3)PbI(3) Perovskite Solar Cells with Suppressed Hysteresis. ACS Appl Mater Interfaces, 2017. 9(40): p. 34833-34843.
75. Wang, J., et al., Room-temperature processed TiO2 to construct composite electron transport layers for efficient planar perovskite solar cells. Journal of Materials Chemistry A, 2023. 11(41): p. 22206-22215.
76. Mufti, N., et al., The enhanced operational stability of perovskite solar cell through low-temperature processed NiO hole transporting layer and GPE passivation. AIP Conference Proceedings, 2023. 2748(1).
77. Yang, G., et al., Interface engineering in planar perovskite solar cells: energy level alignment, perovskite morphology control and high performance achievement. Journal of Materials Chemistry A, 2017. 5(4): p. 1658-1666.
78. Li, Y., et al., Multifunctional Fullerene Derivative for Interface Engineering in Perovskite Solar Cells. Journal of the American Chemical Society, 2015. 137(49): p. 15540-15547.
79. Zhou, Y., et al., Enhancing electron transport via graphene quantum dot/SnO2 composites for efficient and durable flexible perovskite photovoltaics. Journal of Materials Chemistry A, 2019. 7(4): p. 1878-1888.
80. Zhao, Y., et al., Comprehensive Study of Sol–Gel versus Hydrolysis–Condensation Methods To Prepare ZnO Films: Electron Transport Layers in Perovskite Solar Cells. ACS Applied Materials & Interfaces, 2017. 9.
81. Song, J., et al., Low-temperature SnO2-based electron selective contact for efficient and stable perovskite solar cells. Journal of Materials Chemistry A, 2015. 3(20): p. 10837-10844.
82. Ke, W., et al., Low-Temperature Solution-Processed Tin Oxide as an Alternative Electron Transporting Layer for Efficient Perovskite Solar Cells. Journal of the American Chemical Society, 2015. 137(21): p. 6730-6733.
83. Song, J., et al., Efficient and Environmentally Stable Perovskite Solar Cells Based on ZnO Electron Collection Layer. Chemistry Letters, 2015. 44.
84. Feng, X., et al., Defects in Perovskite Solar Cells and Their Passivation Strategies. 2023. 8(45): p. e202302617.
85. Kim, B.J., et al., Highly efficient and bending durable perovskite solar cells: toward a wearable power source. Energy & Environmental Science, 2015. 8(3): p. 916-921.
86. Oviroh, P.O., et al., New development of atomic layer deposition: processes, methods and applications. Science and Technology of Advanced Materials, 2019. 20(1): p. 465-496.
87. Lu, H., et al., Identifying the optimum thickness of electron transport layers for highly efficient perovskite planar solar cells. Journal of Materials Chemistry A, 2015. 3(32): p. 16445-16452.
88. Dong, X., et al., The effect of ALD-Zno layers on the formation of CH3NH3PbI3 with different perovskite precursors and sintering temperatures. Chemical Communications, 2014. 50(92): p. 14405-14408.
89. Lee, Y., et al., Efficient Planar Perovskite Solar Cells Using Passivated Tin Oxide as an Electron Transport Layer. Adv Sci (Weinh), 2018. 5(6): p. 1800130.
90. Vadivel, S. and S. Vadivel, Effect of W doping on structural, optical and photocatalytic activity of SnO2 nanostructure thin films. Journal of Materials Science: Materials in Electronics, 2015. 26.
91. Shin, D., et al., Study of Band Structure at the Zn(S,O,OH)/Cu(In,Ga)Se-2 Interface via Rapid Thermal Annealing and Their Effect on the Photovoltaic Properties. ACS applied materials & interfaces, 2013. 5.
92. Sun, K., et al., Over 9% Efficient Kesterite Cu2ZnSnS4 Solar Cell Fabricated by Using Zn1–xCdxS Buffer Layer. Advanced Energy Materials, 2016. 6(12): p. 1600046.
93. Liu, Z., et al., 15% efficient carbon based planar-heterojunction perovskite solar cells using a TiO2/SnO2 bilayer as the electron transport layer. Journal of Materials Chemistry A, 2018. 6(17): p. 7409-7419.
94. Kumar, M.H., et al., Flexible, low-temperature, solution processed ZnO-based perovskite solid state solar cells. Chemical Communications, 2013. 49(94): p. 11089-11091.
95. Song, J.-X., et al., Low-temperature-processed metal oxide electron transport layers for efficient planar perovskite solar cells. Rare Metals, 2021. 40: p. 2730-2746.

96. Su, T.-S., et al., Electrodeposited Ultrathin TiO2 Blocking Layers for Efficient Perovskite Solar Cells. Scientific Reports, 2015. 5(1): p. 16098.
97. Zhang, J. and T. Pauporté, Effects of Oxide Contact Layer on the Preparation and Properties of CH3NH3PbI3 for Perovskite Solar Cell Application. The Journal of Physical Chemistry C, 2015. 119(27): p. 14919-14928.
98. Chen, J.-Y., et al., Low-temperature electrodeposited crystalline SnO2 as an efficient electron-transporting layer for conventional perovskite solar cells. Solar Energy Materials and Solar Cells, 2017. 164: p. 47-55.
99. Yang, D., et al., High efficiency flexible perovskite solar cells using superior low temperature TiO2. Energy & Environmental Science, 2015. 8(11): p. 3208-3214.
100. Ma, J., et al., Highly Efficient and Stable Planar Perovskite Solar Cells With Large-Scale Manufacture of E-Beam Evaporated SnO2 Toward Commercialization. Solar RRL, 2017. 1(10): p. 1700118.
101. Noman, M., Z. Khan, and S.T.J.R.a. Jan, A comprehensive review on the advancements and challenges in perovskite solar cell technology. 2024. 14(8): p. 5085-5131.
102. Mohammad, A. and F.J.B.J.M.I. Mahjabeen, Promises and challenges of perovskite solar cells: a comprehensive review. 2023. 2(5): p. 1147-1157.
103. Saranya, K. and B.J.J.o.M.S. Janarthanan, Progress and challenges of lead free halide perovskite materials for perovskite solar cell applications. 2023. 1287: p. 135663.
104. Wojciechowski, K., et al., Sub-150 °C processed meso-superstructured perovskite solar cells with enhanced efficiency. Energy & Environmental Science, 2014. 7(3): p. 1142-1147.
105. Conings, B., et al., An easy-to-fabricate low-temperature TiO2 electron collection layer for high efficiency planar heterojunction perovskite solar cells. APL Materials, 2014. 2(8).
106. Tan, H., et al., Efficient and stable solution-processed planar perovskite solar cells via contact passivation. Science, 2017. 355(6326): p. 722-726.
107. Li, Q., et al., Efficient Perovskite Solar Cells Fabricated Through CsCl-Enhanced PbI2 Precursor via Sequential Deposition. Advanced Materials, 2018. 30(40): p. 1803095.
108. Shahiduzzaman, M., et al., Low-temperature treated anatase TiO2 nanophotonic-structured contact design for efficient triple-cation perovskite solar cells. Chemical Engineering Journal, 2021. 426: p. 131831.
109. Yella, A., et al., Nanocrystalline Rutile Electron Extraction Layer Enables Low-Temperature Solution Processed Perovskite Photovoltaics with 13.7% Efficiency. Nano Letters, 2014. 14(5): p. 2591-2596.
110. Liu, X., et al., All low-temperature processed carbon-based planar heterojunction perovskite solar cells employing Mg-doped rutile TiO2 as electron transport layer. 2018. 283: p. 1115-1124.
111. Chen, C., et al., Radio Frequency Magnetron Sputtering Deposition of TiO2 Thin Films and Their Perovskite Solar Cell Applications. Scientific Reports, 2015. 5(1): p. 17684.
112. Mali, S.S., et al., Efficient planar n-i-p type heterojunction flexible perovskite solar cells with sputtered TiO2 electron transporting layers. Nanoscale, 2017. 9(9): p. 3095-3104.
113. Shahiduzzaman, M., et al., Low-temperature treated anatase TiO2 nanophotonic-structured contact design for efficient triple-cation perovskite solar cells. 2021. 426: p. 131831.
114. Lee, J., et al., Compact SnO2/mesoporous TiO2 bilayer electron transport layer for perovskite solar cells fabricated at low process temperature. 2022. 12(4): p. 718.
115. Nam, J., et al., Surface Engineering of Low-Temperature Processed Mesoporous TiO2 via Oxygen Plasma for Flexible Perovskite Solar Cells. ACS Applied Materials & Interfaces, 2020. 12(11): p. 12648-12655.
116. Hwang, K., et al., Toward large scale roll-to-roll production of fully printed perovskite solar cells. Adv Mater, 2015. 27(7): p. 1241-7.
117. Zhou, H., et al., Low-Temperature Processed and Carbon-Based ZnO/CH3NH3PbI3/C Planar Heterojunction Perovskite Solar Cells. The Journal of Physical Chemistry C, 2015. 119(9): p. 4600-4605.
118. Song, J., et al., HC(NH2)2PbI3 as a thermally stable absorber for efficient ZnO-based perovskite solar cells. Journal of Materials Chemistry A, 2016. 4(21): p. 8435-8443.
119. Song, J., et al., Highly efficient and stable low-temperature processed ZnO solar cells with triple cation perovskite absorber. Journal of Materials Chemistry A, 2017. 5(26): p. 13439-13447.
120. Guo, Y., et al., A strategy toward air-stable and high-performance ZnO-based perovskite solar cells fabricated under ambient conditions. Chemical Engineering Journal, 2017. 336.
121. Zhou, J., et al., Low-temperature aqueous solution processed ZnO as an electron transporting layer for efficient perovskite solar cells. Materials Chemistry Frontiers, 2017. 1(5): p. 802-806.
122. Savva, A., I. Burgués-Ceballos, and S.A. Choulis, Improved Performance and Reliability of p-i-n Perovskite Solar Cells via Doped Metal Oxides. Advanced Energy Materials, 2016. 6.
123. Lee, K.-M., et al., Thickness effects of ZnO thin film for tri-iodide perovskite absorber based photovoltaics. Solar Energy, 2015. 120.
124. Tseng, Z.-L., C.-H. Chiang, and C.-G. Wu, Surface Engineering of ZnO Thin Film for High Efficiency Planar Perovskite Solar Cells. Scientific Reports, 2015. 5(1): p. 13211.
125. Tseng, Z.-L., et al., Surface Engineering of ZnO Electron Transporting Layer via Al Doping for High Efficiency Planar Perovskite Solar Cells. Nano Energy, 2016. 28: p. 311-318.
126. Lai, W.-C., et al., Conversion efficiency improvement of inverted CH3NH3PbI3 perovskite solar cells with room

temperature sputtered ZnO by adding the C60 interlayer. Applied Physics Letters, 2015. 107(25).
127. Shekargoftar, M., et al., Low-Temperature and Rapid Deposition of an SnO2 Layer from a Colloidal Nanoparticle Dispersion for Use in Planar Perovskite Solar Cells. 2021. 9(5): p. 2001076.
128. Zuo, L., et al., Polymer-modified halide perovskite films for efficient and stable planar heterojunction solar cells. Science Advances, 2017. 3(8): p. e1700106.
129. Dong, Q., et al., Energetically favored formation of SnO2 nanocrystals as electron transfer layer in perovskite solar cells with high efficiency exceeding 19%. Nano Energy (Print), 2017: p. 336-344.
130. Subbiah, A., et al., Novel Plasma-Assisted Low-Temperature-Processed SnO 2 Thin Films for Efficient Flexible Perovskite Photovoltaics. ACS Energy Letters, 2018. 3.
131. Jiang, Q., et al., Enhanced electron extraction using SnO2 for high-efficiency planar-structure HC(NH2)2PbI3-based perovskite solar cells. Nature Energy, 2016. 2.
132. Jiang, Q., et al., Planar-Structure Perovskite Solar Cells with Efficiency beyond 21%. Advanced Materials, 2017. 29(46): p. 1703852.
133. Jiang, Q., et al., Surface passivation of perovskite film for efficient solar cells. Nature Photonics, 2019. 13(7): p. 460-466.
134. Bu, T., et al., Universal passivation strategy to slot-die printed SnO2 for hysteresis-free efficient flexible perovskite solar module. Nature Communications, 2018. 9(1): p. 4609.
135. Yang, G., et al., Effective Carrier-Concentration Tuning of SnO(2) Quantum Dot Electron-Selective Layers for High-Performance Planar Perovskite Solar Cells. Adv Mater, 2018. 30(14): p. e1706023.
136. Correa Baena, J.P., et al., Highly efficient planar perovskite solar cells through band alignment engineering. Energy & Environmental Science, 2015. 8(10): p. 2928-2934.
137. Wang, C., et al., Low-temperature plasma-enhanced atomic layer deposition of tin oxide electron selective layers for highly efficient planar perovskite solar cells. Journal of Materials Chemistry A, 2016. 4(31): p. 12080-12087.
138. Wang, C., et al., Water Vapor Treatment of Low-Temperature Deposited SnO2 Electron Selective Layers for Efficient Flexible Perovskite Solar Cells. ACS Energy Letters, 2017. 2(9): p. 2118-2124.
139. Anaraki, E.H., et al., Highly efficient and stable planar perovskite solar cells by solution-processed tin oxide. Energy & Environmental Science, 2016. 9(10): p. 3128-3134.
140. Viorica, R.-P., et al., Lactococcus lactis as a safe and inexpensive source of bioactive silver composites. Applied Microbiology and Biotechnology, 2017. 101(19): p. 7141-7153.
141. Liu, X., et al., A Low-Temperature, Solution Processable Tin Oxide Electron-Transporting Layer Prepared by the Dual-Fuel Combustion Method for Efficient Perovskite Solar Cells. Advanced Materials Interfaces, 2016. 3(13).
142. Chen, Z., et al., Bulk heterojunction perovskite solar cells based on room temperature deposited hole-blocking layer: Suppressed hysteresis and flexible photovoltaic application. Journal of Power Sources, 2017. 351: p. 123-129.
143. Kim, S., et al., Effects of potassium treatment on SnO2 electron transport layers for improvements of perovskite solar cells. Solar Energy, 2022. 233: p. 353-362.
144. Huang, L., et al., UV-Sintered Low-Temperature Solution-Processed SnO2 as Robust Electron Transport Layer for Efficient Planar Heterojunction Perovskite Solar Cells. ACS Applied Materials & Interfaces, 2017. 9(26): p. 21909-21920.
145. Dissanayake, S., et al., Facile and low-cost synthesis of pure hematite (α-Fe2O3) nanoparticles from naturally occurring laterites and their superior adsorption capability towards acid-dyes. RSC Advances, 2019.
146. Fouad, D.E., et al., Improved size, morphology and crystallinity of hematite (α-Fe2O3) nanoparticles synthesized via the precipitation route using ferric sulfate precursor. Results in Physics, 2019. 12: p. 1253-1261.
147. Suman, S., et al., Zn Doped α-Fe2O3: An Efficient Material for UV Driven Photocatalysis and Electrical Conductivity. Crystals, 2020. 10: p. 273.
148. Piccinin, S., The band structure and optical absorption of hematite (α-Fe2O3): a first-principles GW-BSE study. Physical Chemistry Chemical Physics, 2019. 21(6): p. 2957-2967.
149. Luan, P., et al., Effective charge separation in the rutile TiO2 nanorod-coupled ??-Fe2O3 with exceptionally high visible activities. Scientific reports, 2014. 4: p. 6180.
150. Guo, Y., et al., Ni-doped α-Fe2O3 as electron transporting material for planar heterojunction perovskite solar cells with improved efficiency, reduced hysteresis and ultraviolet stability. Nano Energy, 2017. 38: p. 193-200.
151. Zhu, W., et al., Non-equilibrium Ti4+ doping strategy for an efficient hematite electron transport layer in perovskite solar cells. Dalton Transactions, 2018.
152. Foo, S., et al., Recent review on electron transport layers in perovskite solar cells. International Journal of Energy Research, 2022. 46(15): p. 21441-21451.
153. Qureshi, A., et al., Solvent-Assisted Crystallization of an α-Fe 2 O 3 Electron Transport Layer for Efficient and Stable Perovskite Solar Cells Featuring Negligible Hysteresis. ACS Omega, 2023. 8.
154. Qureshi, A.A., et al., Low-temperature processed natural hematite as an electron extraction layer for efficient and stable perovskite solar cells. Surfaces and Interfaces, 2023. 40: p. 103003.
155. Humayun, M., et al., Modification strategies of TiO2 for potential applications in photocatalysis: A critical review. Green Chemistry Letters and Reviews, 2018. 2: p. 86-102.

156. Wang, K., et al., W(Nb)Ox-based Efficient Flexible Perovskite Solar Cells: From Material Optimization to Working Principle. Nano Energy, 2016. 31.
157. Shin, S.S., et al., High-performance flexible perovskite solar cells exploiting Zn2SnO4 prepared in solution below 100 °C. Nat Commun, 2015. 6: p. 7410.
158. Shin, S.S., et al., Tailoring of Electron-Collecting Oxide Nanoparticulate Layer for Flexible Perovskite Solar Cells. The Journal of Physical Chemistry Letters, 2016. 7(10): p. 1845-1851.
159. Jung, K., et al., Highly Efficient Amorphous Zn 2 SnO 4 Electron-Selective Layers Yielding over 20% Efficiency in FAMAPbI 3 -Based Planar Solar Cells. ACS Energy Letters, 2018. 3: p. 2410-2417.
160. Zhu, L., et al., Performance enhancement of perovskite solar cells using a La-doped BaSnO3 electron transport layer. Journal of Materials Chemistry A, 2017. 5(7): p. 3675-3682.
161. Shin, S.S., et al., Colloidally prepared La-doped BaSnO(3) electrodes for efficient, photostable perovskite solar cells. Science, 2017. 356(6334): p. 167-171.
162. Liu, S., et al., An intermeshing electron transporting layer for efficient and stable CsPbI2Br perovskite solar cells with open circuit voltage over 1.3 V. Journal of Materials Chemistry A, 2020. 8(29): p. 14555-14565.
163. Wang, K., et al., Amorphous Inorganic Electron-Selective Layers for Efficient Perovskite Solar Cells: Feasible Strategy Towards Room-Temperature Fabrication. Advanced Materials, 2016. 28(9): p. 1891-1897.
164. Song, J., et al., Low-temperature-processed ZnO–SnO2 nanocomposite for efficient planar perovskite solar cells. Solar Energy Materials and Solar Cells, 2016. 144: p. 623–630.